Ultrafast Two-Dimensional Infrared Vibrational Echo Chemical Exchange Experiments and Theory†

Kyungwon Kwak, Junrong Zheng, Hu Cang, and M. D. Fayer*

Department of Chemistry, Stanford University, Stanford, California 94305

Received: April 22, 2006; In Final Form: July 12, 2006

Ultrafast two-dimensional (2D) infrared vibrational echo experiments and theory are used to examine chemical exchange between solute−solvent complexes and the free solute for the solute phenol and three solvent complex partners, *p*-xylene, benzene, and bromobenzene, in mixed solvents of the partner and CCl_4. The experiments measure the time evolution of the 2D spectra of the hydroxyl (OD) stretching mode of the phenol. The time-dependent 2D spectra are analyzed using time-dependent diagrammatic perturbation theory with a model that includes the chemical exchange (formation and dissociation of the complexes), spectral diffusion of both the complex and the free phenol, orientational relaxation of the complexes and free phenol, and the vibrational lifetimes. The detailed calculations are able to reproduce the experimental results and demonstrate that a method employed previously that used a kinetic model for the volumes of the peaks is adequate to extract the exchange kinetics. The current analysis also yields the spectral diffusion (time evolution of the dynamic line widths) and shows that the spectral diffusion is significantly different for phenol complexes and free phenol.

I. Introduction

In this paper ultrafast two-dimensional (2D) infrared vibrational echo experiments that measure the formation and dissociation of solute−solvent complexes on a picosecond time scale under thermal equilibrium conditions are presented, and the theoretical underpinnings of such experiments are laid out in detail. Recent papers on solute−solvent chemical exchange experiments employed a kinetic scheme to analyze the data that included orientational relaxation rates, vibrational lifetimes, and an indirect accounting for spectral diffusion,[1,2] but the fundamental nature of the experiments, including the multiple light−matter interactions and how they relate to the experimental observables, was not treated.

Chemical exchange reactions on the picosecond time scale include intermolecular exchange, isomerization, proton transfer, and electron transfer. Intermolecular exchange, discussed here, is important in chemistry and biology. It forms the basis for supramolecular chemistry,[3] host−guest chemistry,[3] chemical and biological recognition,[4] and self-assembly.[3] Specific intermolecular interactions, such as hydrogen bonding, can lead to structurally unique solute−solvent complexes that are constantly forming and dissociating under thermal equilibrium conditions on very short time scales.[1,2,5] Dynamics of these transient species play a role in the physical and chemical properties of solute−solvent systems by affecting reaction rates, reaction mechanisms, and product ratios.[6] Although solute−solvent chemical exchange experiments will be discussed here, the theoretical description of the 2D IR vibrational echo chemical exchange experiment is applicable to all types of chemical exchange phenomena.

Until recently, chemical exchange on the picosecond time scale could not be measured under thermal equilibrium conditions. Two IR methods, 2D IR heterodyne-detected vibrational echoes[1,2,7,8] and two color IR pump−probe experiments,[9] can be used. The 2D vibrational echo method explicated here has some advantages that generally accrue to Fourier transform spectroscopies, but more important, it does not have the time-bandwidth limitations of narrow band pump/broad band probe experiments.

There are methods that can measure chemical exchange for reactions slower than 10^{-10} s.[10] For reactions in the 10^{-12} s range, line shape analysis of linear-IR and Raman vibrational spectra has been used,[11] but line shape analysis is fraught with difficulties because of the multiple dynamic processes that can contribute to the line shape in addition to exchange.[12−14]

Two-dimensional NMR provides an excellent method for studying chemical exchange on time scales of microseconds or longer.[15−17] However, for solute−solvent complexes in organic and other types of nonaqueous solutions that are of interest here, the complexes are bound by energies on the order of a few *RT* ($RT \approx 0.6$ kcal/mol at room temperature, where *R* is the gas constant) and, therefore, form and dissociate on very rapidly. The 2D IR vibrational echo chemical exchange technique[1,2,7,8] is the ultrafast analogue of 2D NMR chemical exchange spectroscopy.[15−17] Both the 2D NMR and the 2D vibrational echo techniques involve pulse sequences that induce and then probe the coherent evolution of excitations (nuclear spins for NMR and vibrations for IR) of a molecular system. In the 2D vibrational echo experiment, a selected molecular vibration of molecules in a given environment (for example, a free solute versus complexed solute) is placed in a coherent superposition state by the first pulse in the sequence. The effect of the first pulse and the manipulation of the phase relationships among the excitations by the following pulses in the sequence is an important common feature of 2D vibrational echo spectroscopy and 2D NMR. The later pulses generate observable signals that are sensitive to chemical exchanges. The critical difference between the IR and NMR variants is that the IR pulse sequence acts on a time scale 6−9 orders of magnitude faster than the radio frequency pulse sequence in NMR.

† Part of the special issue "Charles B. Harris Festschrift".

* Author to whom correspondence should be addressed. E-mail: fayer@stanford.edu.

10.1021/jp0624808 CCC: $33.50
Published on Web 08/30/2006

Vibrational-echo-based 2D IR experiments have been applied to a wide variety of problems, and both experiment and theory have been presented.[18−29] However, its application to chemical exchange is quite new,[1,2,7,8] and a full theoretical description with comparisons to experiments has not been given. Previously, data for the solute phenol complexed with benzene in a mixed solvent of benzene and CCl_4 was presented.[1] More recently, solute−solvent chemical exchange for the solute 2-methoxyphenol was published.[2] Here, the phenol/benzene data along with the phenol/*p*-xylene and phenol/bromobenzene data will be analyzed in detail using time-dependent diagrammatic perturbation theory[30] and a model that includes chemical exchange, spectral diffusion, orientational relaxation, and the vibrational lifetimes. The model is able to describe the data extremely well. One of the important results is that the detailed theory presented here confirms that the much simpler method of analysis used previously[1,2] is sufficient to extract the exchange kinetics. Application of the full theory also provides details of the spectral diffusion for the complexed and free phenol.

In the experiments presented below, a solute, phenol-OD (hydroxyl hydrogen replaced by a deuterium, which will be referred to as phenol for simplicity) exists in equilibrium as a complex with benzene (or *p*-xylene or bromobenzene) or as the free uncomplexed form. There are two peaks in the linear Fourier transform IR spectrum, one for the complex and one for the free species.[1] In the 2D IR vibrational echo spectrum at very short time (small interval between pulses 2 and 3 in the pulse sequence, see below) there are two peaks on the diagonal, one for the complex and one for free phenol. As time is increased, complexes form and dissociate under thermal equilibrium conditions. The chemical exchange produces off-diagonal peaks, which increase as time is increased. If no other processes occurred, then the growth in amplitude of the off-diagonal peaks would be simply related to the rate of the chemical exchange rate, that is the rate of complex formation and dissociation, which are equal for an equilibrium system.[1] However, spectral diffusion causes the peaks to change shape, and therefore, the peak heights cannot be used to analyze the data. In addition, orientational relaxation causes all peaks to decrease in amplitude. Because, in general, the orientational relaxation rates of the two species are not the same, the orientational relaxation with different rates for the species that are interconverting must be taken into account in the theoretical analysis. The species are also undergoing vibrational population relaxation (T_1), which decreases all peaks as time increases. Again, the lifetimes of the species are not the same, and the lifetimes with the species interconverting must be properly accounted for in the theoretical analysis. Another important feature of the problem is that the species, complexed and free phenol, do not have the same transition dipole matrix elements. All of these properties of the physical system are accounted for in the theoretical development presented below.

II. Experimental Procedures

A. Sample Preparation. Phenol forms weak complexes with benzene and its derivatives.[1,4,31,32] The polar hydroxyl group on phenol (OD in these experiments) and polarizable π-electron cloud of benzene lead to the attraction between these molecules. The resulting weak hydrogen bond that forms the complex shifts the OD stretching frequency to a lower frequency than that in the non-hydrogen-bonded free phenol. Phenol was deuterated by deuterium exchange with methanol-OD. In pure benzene solvent, only one OD stretch peak, corresponding to the complex, is observed, although there is a low-amplitude, high-frequency tail that corresponds to free phenol.[1] To observe the formation and dissociation of the phenol−benzene complex, a mixed solvent of benzene and CCl_4 was used to shift the equilibrium to more of the free species. In pure CCl_4, only the free species is present. The free phenol has a higher-frequency hydroxyl stretch because of the lack of the hydrogen bond. Infrared spectra of free phenol in pure CCl_4, phenol−benzene complex in pure benzene, and phenol−benzene complex and free phenol in the benzene/CCl_4 mixed solvent have been published.[1] The spectra in the mixed solvents for the three systems studied here are shown in Figures 3a, 5a, and 7a. The mixed solvent creates a well-defined double potential minimum with similar populations along the exchange coordinate.

B. Optical System and Methodology. The ultrashort IR pulses (∼50 fs) employed in the experiments were generated using a Ti:sapphire regeneratively amplified laser/optical parametric amplifier (OPA) system. The output of the regen is 40 fs transform-limited $^2/_3$ mJ pulses at a 1 kHz repetition rate. These are used to pump the short-pulse IR OPA. The output of the OPA is compressed to produce 50 fs transform-limited IR pulses in the actual sample cell using a purely nonresonant signal and frequency-resolved optical grating (FROG)[33] measurements. The pulses span sufficient bandwidth (300 cm^{-1} centered at 2500 cm^{-1}) to cover the $\upsilon = 0$ to $\upsilon = 1$ (hereafter denoted 0−1) and 1−2 transitions of the hydroxyl OD stretching modes in both free and complexed phenol.

The compressed IR output of the OPA is split into five beams. Three equal-intensity IR pulses impinge on the sample and stimulate the emission of the vibrational echo, a pulse that leaves the sample in a unique direction at a time following the third pulse. Another beam is made collinear with the vibrational echo path through the sample. It is used only for alignment and is blocked during the actual experiments. A fifth pulse, the local oscillator, does not pass through the sample and is overlapped with the vibrational echo pulse for heterodyne detection of the echo. The combined vibrational echo/local oscillator beam is directed into a spectrograph, and the spectrally dispersed signal is measured using a 32 element mercury cadmium telluride (MCT) array to record 32 frequencies simultaneously. The center frequency of the spectrograph is moved to record sets of 32 frequencies to span the entire spectrum.

The frequency- and phase-resolved, stimulated vibrational echo is measured as a function of one frequency variable from the spectrograph, ω_m, and two time variables, τ and T_w, the time between the first and second and the second and third IR pulses, respectively. ω_m provides one frequency axis of the 2D vibrational echo spectrum. By numerical Fourier transformation, the τ scan data are converted into the second frequency variable, providing the ω_τ axis. The resulting interferogram contains both the absorptive and the dispersive components of the vibrational echo signal.[34] To greatly reduce the dispersive contribution and obtain close to pure absorptive features, two sets of quantum pathways are measured independently by appropriate time ordering of the pulses in the experiment.[34] With pulses 1 and 2 at the time origin, pathway 1 or 2 is obtained by scanning pulse 1 or 2 to negative time, respectively. By addition of the Fourier transform of the combined interferograms from the two pathways, the dispersive component is substantially eliminated, which greatly narrows the features in the spectra. The 2D IR vibrational echo spectra are constructed by plotting the amplitude of the nominally absorptive part of the vibrational echo as a function of both ω_m and ω_τ. Additional experimental details, including procedures to ensure that phase relationships in the spectrum are proper, are discussed elsewhere.[35]

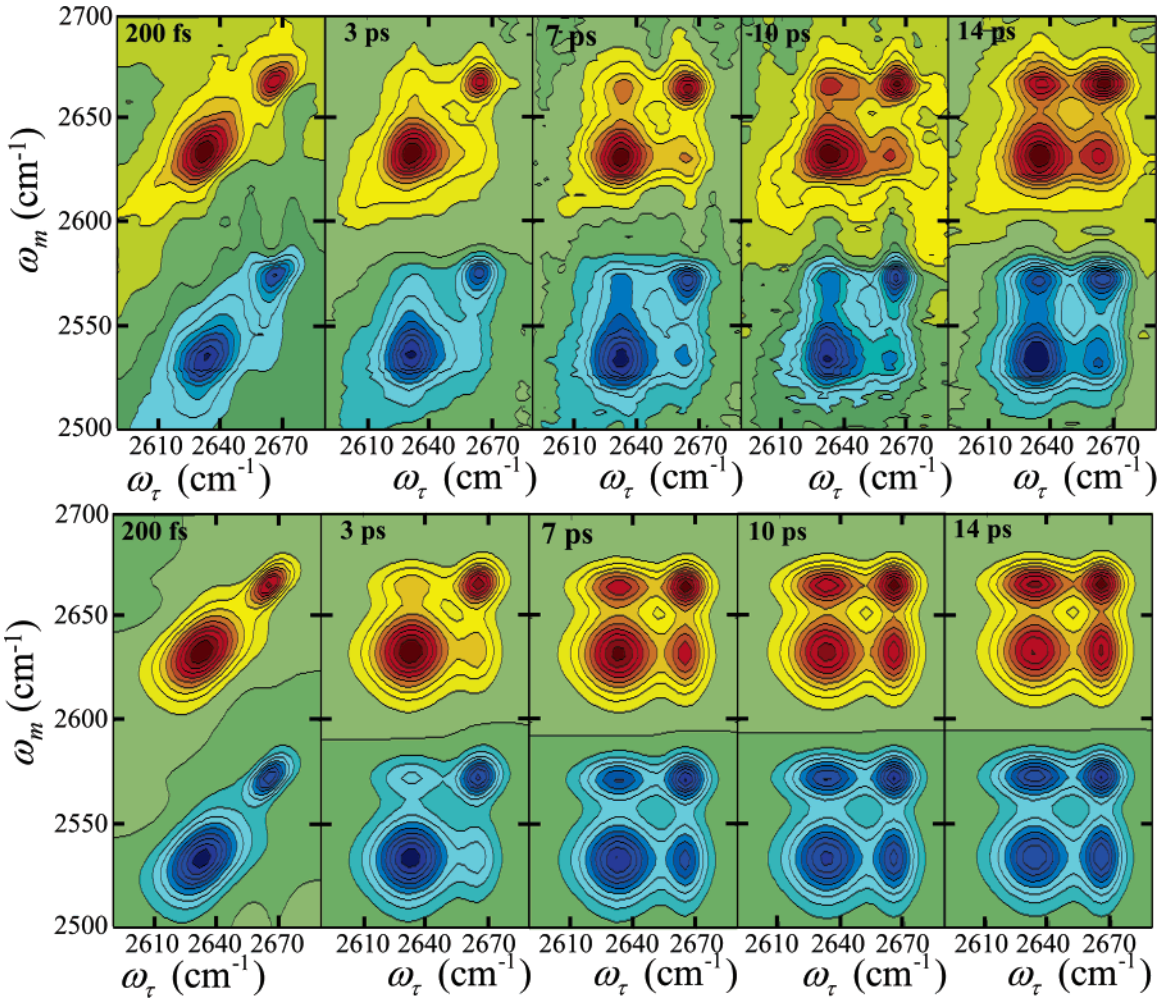

Figure 1. T_w-dependent 2D IR vibrational echo spectra (top) of the hydroxyl stretch of phenol-OD in benzene/CCl_4 mixed solvents (molar ratio of phenol/benzene/CCl_4 = 2:40:100). The red peaks (positive) are from the 0−1 vibration transitions, and the blue peaks (negative) are from the 1−2 vibrational transitions. At 200 fs, there are two peaks on the diagonal (red) and two peaks below these (blue) shifted by the anharmonicity. As T_w increases, additional peaks appear due to chemical exchange, that is, dissociation and formation of the phenol−benzene complex. The bottom portion displays response function calculations of the data as discussed in section V.

The dual-scan method can remove a substantial portion of the dispersive contributions to the 2D spectrum. In a 2D vibrational echo spectrum of two or more modes of a molecule with intramolecular coupling between them, there is an inherent imbalance of interaction pathways that results in substantial uncanceled dispersive contributions that are greater for the off-diagonal peaks than for the diagonal peaks.[28,34] However, there is no imbalance of interaction pathways in any of the peaks produced by the exchange process as shown by the Feynman pathways (see below). There are the same numbers of non-rephasing and rephrasing pathways for each peak. Therefore, the dual-scan method can, to a large extent, remove dispersive contributions to all peaks in the 2D spectrum if the off-diagonal peaks are produced solely by exchange. The phasing procedure using the projection theorem was applied,[35,36] and correctly phased diagonal and off-diagonal peaks were obtained.

III. Results

Figure 1 (top portion) displays the 2D IR vibrational echo spectra as contour plots (each contour is a 10% change) at various T_w points (from 200 fs to 14 ps) for the phenol−benzene complex system. (Two-dimensional data for the other systems are shown in Figures 4a and 6a.) The data have been normalized to the largest peak at each T_w. The red contours are positive going (0−1 vibrational transition), and the blue contours are negative going (1−2 vibrational transition). The 0−1 signal comes from two quantum pathways that are related to bleaching of the ground state and stimulated emission, both of which produce a vibrational echo pulse that is in phase with and therefore adds to the local oscillator pulse to produce a positive going signal. The 1−2 signal arises because there is a new absorption that was not present prior to the first two excitation pulses. The 1−2 vibrational echo pulse is 180° out of phase with the local oscillator and thus subtracts from the local oscillator to produce a negative going signal. At T_w = 200 fs, there are two peaks on the diagonal (0−1 transitions) and the corresponding 1−2 transition peaks off-diagonal. As T_w (waiting time) is increased, the off-diagonal peaks of the 0−1 transition and the corresponding 1−2 peaks appear.

There are a number of phenomena that can produce off-diagonal peaks. Two coupled modes on the same molecule will have the peaks for each mode on the diagonal and coherence transfer peaks off-diagonal.[28] In addition there will be negative going peaks off-diagonal below the coherence transfer peaks. These peaks are present at T_w = 0 and do not increase in amplitude. It is possible to have incoherent population relaxation between two modes on the same molecule that are coupled by anharmonic terms in the molecular potential. Such population relaxation will produce off-diagonal peaks that appear with increasing T_w.[37] However, the two modes have to be on the

same molecule and within the laser bandwidth. As shown by the linear spectroscopy, the phenol system has a single OD stretch.[1] It has one frequency when it is free and another when it is a complex. The two frequencies correspond to the complex and free phenol peaks. Therefore, each species has a single mode, and population relaxation between modes cannot be responsible for the growth of the off-diagonal peaks. Vibrational Förster excitation transfer can transfer a vibrational excitation between modes on distinct molecules.[38,39] However, this is extremely short range because of very small vibrational transition dipoles and short vibrational lifetimes, with a range of 2−3 Å for hydroxyl stretches.[39] Given the low concentration of the complex and free phenol in the solution, Förster transfer is not a possibility.

The linear spectroscopy of the species, the temperature dependence of the spectra, and electronic structure calculations that show that the complex is stable, combined with the growth of the off-diagonal peaks, demonstrate that chemical exchange between complexed and free phenol is being observed.[1] Through the use of time-dependent diagrammatic perturbation theory, which describes nonlinear optical interactions with the molecular vibrations,[40,41] the chemical exchange experiments can be described quantitatively. It is necessary to include in the calculations not only chemical exchange but also orientational relaxation of each species, vibrational relaxation of each species, and the differences in the transition dipole moment matrix elements of the species. The detailed theory will be presented in the next section. First a brief description of the origin of the off-diagonal peaks will be given to set a qualitative stage for the detailed theoretical description.

The frequency at which the first pulse excites a mode is the mode frequency on the ω_τ axis (horizontal axis), 2631 cm^{-1} for the 0−1 transition in complex and 2665 cm^{-1} for the free phenol. The third pulse causes a mode to emit the time-delayed vibrational echo pulse at the frequency of the third interaction (third pulse) of the radiation field with the mode. The frequency of the vibrational echo emission is the frequency on the ω_m axis (the vertical axis). First consider $T_w = 200$ fs in Figure 1 in which the data are taken on a short time scale in comparison to the rate of chemical exchange. For the 0−1 vibrational transitions, the third pulse induces the vibrational echo emission at the same frequencies excited by the first pulse, so there are two peaks on the diagonal where $\omega_\tau = \omega_m$ (red peaks in Figure 1). If the frequency of vibrational echo emission (ω_m, third interaction frequency) is different from the frequency of initial excitation (ω_τ, first interaction frequency), then the peaks will appear off-diagonal. Again, for $T_w = 200$ fs in Figure 1, the blue peaks are off-diagonal by the vibrational anharmonicity because the modes are initially excited at their 0−1 frequencies (ω_τ), but the third pulse causes vibrational echo emission at their 1−2 frequencies (ω_m). Even in the absence of chemical exchange, the peaks observed at very short T_w delays undergo evolution with increasing T_w, because of spectral diffusion, which changes the shapes of the peaks, and vibrational lifetime decay and orientational relaxation, which cause the peaks to decay in amplitude.

The influence of chemical exchange on the 2D correlation spectrum can be understood qualitatively as follows. After the first two pulses in the vibrational echo sequence, if some of the complexed phenols dissociate during the T_w period, then the third pulse will cause the emission of the vibrational echo at the frequency of the free phenol OD stretch for these newly dissociated phenols. The frequency of emission, ω_m, then differs from the excitation frequency, ω_τ, for these specific molecules. The result will be an off-diagonal peak that only appears if chemical exchange occurs. Because the free phenol absorbs at higher frequency than complexed phenol, this off-diagonal peak is shifted from the complexed phenol frequency to higher frequency along the ω_m axis by the frequency difference (34 cm^{-1}) between the free and the complexed modes. Conversely, if during the T_w period some free phenols associate with benzene, then the third pulse will produce an off-diagonal peak for these (formerly) free phenols, shifted to lower frequency along the ω_m axis by the same amount. Identical considerations apply for both the 0−1 and the 1−2 regions of the spectrum. This behavior is shown in Figure 1 at $T_w = 14$ ps, where substantial chemical exchange has led to the generation of a block of 4 red peaks and a block of 4 blue peaks; the two new peaks in each block were not present at $T_w = 200$ fs. Some complexes have dissociated, and others have formed. The growth of the off-diagonal peaks with increasing T_w is directly related to the time dependence of the chemical exchange.

The description given above and treated below applies for moderate or slow exchange. Fast exchange occurs when the time to jump to a new species and then jump back is comparable to or fast compared to the inverse of the frequency difference between the two peaks.[12,42,43] This in not the case for the systems studied here. In the fast exchange limit, the vibrational linear absorption spectrum will show a single peak.[14,42,43] The 2D IR vibrational echo spectrum will show a single peak on the diagonal; off-diagonal peaks will not appear to provide information on the rate of chemical exchange.

IV. Theory

In the analysis of solute−solvent complex chemical exchange data presented previously,[1,2] a kinetic model was used to fit the data and extract the exchange rate. The model did not explicitly deal with spectral diffusion but took it into account by fitting the time dependence of the peak volumes rather than the peak amplitudes. Orientational relaxation, vibrational lifetimes, and differences in transition dipoles were included. Here, diagrammatic perturbation theory methodology for this problem will be developed and applied. Spectral diffusion is included explicitly and analyzed. One of the important results in addition to obtaining the time dependence of the spectral diffusion is the demonstration that the much simpler kinetic model is accurate if only the chemical exchange is of interest.

In NMR, exchange effects have been studied extensively in both 1D and 2D spectroscopies.[15,17,42,43] Aspects of the NMR theoretical description of chemical exchange can be applied to the current problem so long as the important differences between the NMR problem and the vibrational problem are dealt with. The theoretical treatment includes the effects of chemical exchange during evolution and detection periods. The exchange during the first coherence period does not contribute to the growth of the off-diagonal peaks because the exchange time is long compared to the inverse frequency difference of the peaks (slow to moderate exchange limit). Then, during the first coherence period, jumps from the complex to free form or vice versa will produce ensembles of superposition states in both forms with random phases resulting in no contribution to the off-diagonal peaks. Such jumps do produce dynamic line broadening of the diagonal peaks, which is included in the treatment. Therefore, only exchange during the population period (time between pulses 2 and 3, T_w) contributes to the growth of the off-diagonal peaks.

Spectral diffusion is slow enough that at least for the jumps that occur at short times the lines are inhomogeneously broadened. In the model presented here, it is assumed that there is no correlation in the frequency prior to a jump with the frequency following a jump between species. That is, the species prior to a jump has some position in its inhomogeneous line. After the jump, it can be anywhere in the new line only weighted by the line shape. This is a very reasonable assumption given the nature of the system in which complexes form and dissociate. The ramifications of the lack of correlation will be described below. It is possible to extend the formalism presented here to include frequency correlation, which has been observed in a different type of system.[44]

The processes other than chemical exchange can be divided into two groups. One is the spectral diffusion, which changes the shapes of peaks. The others are the finite lifetimes of excited states and orientational relaxation, both of which diminish the size of the peaks. In NMR, the coupled equations for exchange and population relaxation were derived.[45] The equation of motion of the density matrix for the spin system includes population relaxation via a Redfield-type matrix and exchange via a Kubo−Sack matrix.[46,47] To describe the vibrational problem, orientational relaxation must also be included. Vibration and rotation are generally separated in the theoretical description of vibrational spectroscopy.[48] This separation will be used here during the coherence periods. However, the dynamic partition model can avoid this separation of vibrational motion and rotation during the population period. As described above, the off-diagonal peaks are the result of an exchange process during the population period. Thus, it is important to properly treat various dynamic processes during the population period to accurately extract information about chemical exchange from 2D IR vibrational echo spectra.

Recently, theoretical descriptions of third-order response functions with exchange were published by two groups. Mukamel and co-workers used a Stochastic Liouville Equation[40] to simulate the vibrational echo spectrum of water with a four-site exchange model. Cho and co-workers derived analytical expressions for linear and third-order response functions using a two-species model with exchange and more importantly showed that the truncated cumulant expansion can be used in this two-species model.[41] In their response functions, the exchange effect was inserted using conditional probabilities that describe the probability of each pathway occurring at different T_w values. Both groups use molecular dynamics (MD) simulations to obtain information about exchange rates. Through the analysis of MD trajectories and using appropriate criteria for hydrogen-bonding configurations, species with different hydrogen bond structures were separated. From this separation, the exchange time and lifetime of each species were determined. In these theoretical treatments, the exchange time scale is much faster than vibrational and rotational relaxation time scales, so it was safely assumed that exchange had the dominant effect on the population dynamics; the other factors were not included.

However, in general chemical exchange, orientational relaxation and population relaxation can all occur on similar time scales. This is the situation for the experiments on organic solute−solvent chemical exchange analyzed below and presented previously.[1,2,7] As a result, a theoretical treatment that includes all aspects of the problem that influence the 2D spectrum is required. In the following, first the method for treating the orientational relaxation will be presented. Then, this method will be used with the third-order response functions to obtain a model that describes the chemical exchange problem including spectral diffusion, orientational relaxation, and vibrational population decay. This modified response function approach is used to fit the experimental results with the exchange rate as a parameter as well as a form for the frequency−frequency correlation function (FFCF),[30] which yields a description of the spectral diffusion. Because the vibrational lifetimes and orientational relaxation rates are measured independently using IR pump−probe experiments, these are not adjustable parameters in the fits to the data. The exchange rate and the spectral diffusion have very different effects on the 2D vibrational echo spectra. Therefore, these can be determined with confidence independently from each other. Finally, it will be shown that the simple peak volume fitting approach is sufficient to determine the exchange rate if information on spectral diffusion is not desired.

A. Dynamic Partition Model. During the population period, molecules will experience three different processes that affect the population and finally determine the signal size. As explained above, three different processes include vibrational relaxation, orientational relaxation, and exchange between different species. All three relaxation processes are coupled in this treatment. The contribution of each relaxation process is schematically illustrated as

$$\xleftarrow[\text{decay}]{\tau_r^c, T_1^c} \text{c} \underset{k_{fc}}{\overset{k_{cf}}{\rightleftharpoons}} \text{f} \xrightarrow[\text{decay}]{\tau_r^f, T_1^f}$$

where $\tau_r{}^i = 1/6D_i$ and $T_1{}^i = 1/k_i$ are the orientational relaxation time constant (D_i is the orientational diffusion constant) and the vibrational lifetime of the ith species, respectively, and k_{cf} and k_{fc} are the complex dissociation (complex to free) and formation (free to complex) rate constants, respectively. In the treatment given below, what we refer to as effective populations are calculated. While the vibrational lifetimes and exchange can cause changes in the number of molecules of a given species, orientational relaxation can occur with no change in actual population. However, randomization of the transition dipole direction following interactions with the radiation fields reduces the signals for the diagonal and off-diagonal peaks. Thus, a population's contribution to the signal of a given peak is in some sense a vector quantity, including the magnitude and the projection of the transition dipole on the radiation field direction. These quantities are the effective populations that give rise to the diagonal and off-diagonal peaks.

Because the molecules (complex or free) have initial random orientations, signal size at a frequency ω_m (the frequency of the third interaction producing the coherence and echo emission at that frequency) is proportional to the orientational ensemble average of the population with the coherence frequency of each population

$$I_i(\omega_m = \omega_i) \propto \langle N_i(t) \cos^2 \theta \rangle_i \quad (i = \text{c,f}) \tag{1}$$

Here the orientational ensemble average is defined as

$$\langle \cos^2 \theta \rangle_i = \int_0^{\pi/2} \sin(\theta)\, d\theta\, f_i(\theta) \cos^2(\theta) \tag{2}$$

$f_i(\theta)$ is the angular distribution function for the complex ($i = \text{c}$) and free ($i = \text{f}$) forms.

These effective populations (before the orientational ensemble average of the populations) will evolve as

$$\frac{\mathrm{d}}{\mathrm{d}t}\begin{pmatrix} N_{\mathrm{f}}(t)f_{\mathrm{f}}(\theta,t) \\ N_{\mathrm{c}}(t)f_{\mathrm{c}}(\theta,t) \end{pmatrix} = \begin{pmatrix} -(k_{\mathrm{f}} + k_{\mathrm{fc}} + D_{\mathrm{f}}I^2) & k_{\mathrm{cf}} \\ k_{\mathrm{fc}} & -(k_{\mathrm{c}} + k_{\mathrm{cf}} + D_{\mathrm{c}}I^2) \end{pmatrix}\begin{pmatrix} N_{\mathrm{f}}(t)f_{\mathrm{f}}(\theta,t) \\ N_{\mathrm{c}}(t)f_{\mathrm{c}}(\theta,t) \end{pmatrix} \quad (3)$$

D_{f} and D_{c} are the orientational diffusion constants for the complex and free forms, which in general are not equal. I^2 is the spherical operator. Its eigenfunctions are the spherical harmonics, $Y_m{}^l$. As indicated by the use of diffusion constants, we make the reasonable assumption that the orientational relaxation is diffusive and described by[49]

$$\frac{\partial}{\partial t}f(\theta,t) = -DI^2 f(\theta,t) \quad (4)$$

The formal solution of the coupled differential equations can be written in matrix form as

$$\begin{pmatrix} N_{\mathrm{f}}(t)f_{\mathrm{f}}(\theta,t) \\ N_{\mathrm{c}}(t)f_{\mathrm{c}}(\theta,t) \end{pmatrix} = \exp\left[\begin{pmatrix} -(k_{\mathrm{f}} + k_{\mathrm{fc}} + D_{\mathrm{f}}I^2) & k_{\mathrm{cf}} \\ k_{\mathrm{fc}} & -(k_{\mathrm{c}} + k_{\mathrm{cf}} + D_{\mathrm{c}}I^2) \end{pmatrix}t\right] \times \begin{pmatrix} N_{\mathrm{f}}(0)f_{\mathrm{f}}(\theta,0) \\ N_{\mathrm{c}}(0)f_{\mathrm{c}}(\theta,0) \end{pmatrix} \quad (5)$$

with the boundary conditions of the angular distribution function $f_i(\theta,0)$

$$f_i(\theta,0) = 3\cos^2(\theta)$$
$$f_i(\theta,\infty) = 1 \quad (6)$$

The boundary condition given in eq 6 needs to be discussed in some detail. This boundary condition is correct for pump−probe and fluorescence measurements because there is only one excitation pulse rather than two pulses with a time delay to produce a population in the vibrational echo experiments. Therefore, orientation relaxation should be considered during the coherence period (the period τ between the first and second pulses). The orientational relaxation part for the third-order experiment can be described using the probability evolution Green's function that satisfies the diffusion equation. The result can be expressed as the product of two first-order Legendre polynomials and one second-order Legendre polynomial. The former one describes the orientational relaxation during the two coherence periods and the latter one for population period. Through the use of this result, orientational relaxation for the vibrational echo experiment can be described as

$$R_{ZZZZ} = \frac{1}{9}C_1(t_1)\left(1 + \frac{4}{5}C_2(t_2)\right)C_1(t_3)$$
$$C_l(t_i) = \exp[-l(l+1)Dt_i] \quad (7)$$

Because of the orientational relaxation during first coherence period, the initial condition of $f_i(\theta,0)$ (eq 6) is not exactly $3\cos^2\theta$. However, orientational relaxation during the first coherence period has a decay constant that is a factor of 3 smaller than the decay constant during the population period because of the difference in the coefficient $l(l+1)$. Furthermore, the coherence period is relatively short, ~1 ps, compared to the $C_1(t)$ relaxation time for these experiments (~9 ps). Therefore, we assume that the initial condition given in eq 6 is a reasonable approximation for the initial orientational state at the beginning of the population period. With this assumption, $f_i(\theta,0)$ can be expanded in terms of the spherical harmonics as

$$f_i(\theta,0) = 3\cos^2(\theta) = 2\sqrt{\frac{4\pi}{5}}Y_{20} + \sqrt{4\pi}\,Y_{00} \quad (8)$$

The orientational relaxation during the coherence periods is handled in the conventional manner as exponential decays that multiply the response function (see below). However, because chemical exchange produces the growth of the off-diagonal, it is necessary to explicitly account for jumps back and forth between the two species that are undergoing orientational relaxation at different rates.

Through the use of this initial condition, eq 5 can be solved

$$\begin{pmatrix} N_{\mathrm{f}}(t)f_{\mathrm{f}}(\theta,t) \\ N_{\mathrm{c}}(t)f_{\mathrm{c}}(\theta,t) \end{pmatrix} = \exp\left[\begin{pmatrix} -(k_{\mathrm{f}} + k_{\mathrm{fc}} + 6D_{\mathrm{f}}) & k_{\mathrm{cf}} \\ k_{\mathrm{fc}} & -(k_{\mathrm{c}} + k_{\mathrm{cf}} + 6D_{\mathrm{c}}) \end{pmatrix}t\right] \times \begin{pmatrix} N_{\mathrm{f}}(0) \\ N_{\mathrm{c}}(0) \end{pmatrix}2\sqrt{\frac{4\pi}{5}}Y_{20} + \exp\left[\begin{pmatrix} -(k_{\mathrm{f}} + k_{\mathrm{fc}}) & k_{\mathrm{cf}} \\ k_{\mathrm{fc}} & -(k_{\mathrm{c}} + k_{\mathrm{cf}}) \end{pmatrix}t\right]\begin{pmatrix} N_{\mathrm{f}}(0) \\ N_{\mathrm{c}}(0) \end{pmatrix}\sqrt{4\pi}Y_{00} \quad (9)$$

When the orientational ensemble average is performed, the result is

$$\begin{pmatrix} \langle N_{\mathrm{f}}(t)f_{\mathrm{f}}(\theta,t)\rangle \\ \langle N_{\mathrm{c}}(t)f_{\mathrm{c}}(\theta,t)\rangle \end{pmatrix} = \exp\left[\begin{pmatrix} -(k_{\mathrm{f}} + k_{\mathrm{fc}} + 6D_{\mathrm{f}}) & k_{\mathrm{cf}} \\ k_{\mathrm{fc}} & -(k_{\mathrm{c}} + k_{\mathrm{cf}} + 6D_{\mathrm{c}}) \end{pmatrix}t\right] \times \begin{pmatrix} N_{\mathrm{f}}(0) \\ N_{\mathrm{c}}(0) \end{pmatrix}\frac{4}{15} + \exp\left[\begin{pmatrix} -(k_{\mathrm{f}} + k_{\mathrm{fc}}) & k_{\mathrm{cf}} \\ k_{\mathrm{fc}} & -(k_{\mathrm{c}} + k_{\mathrm{cf}}) \end{pmatrix}t\right]\begin{pmatrix} N_{\mathrm{f}}(0) \\ N_{\mathrm{c}}(0) \end{pmatrix}\frac{1}{3} \quad (10)$$

Equation 10 can be solved analytically using the methods devised by Putzer.[50] The solutions to eq 10 yield both the diagonal and the off-diagonal solutions. The ensemble-averaged solutions for the diagonal peaks are labeled $N_{\mathrm{ff}}(t)$ and $N_{\mathrm{cc}}(t)$, indication that a species began and ended the pulse sequence in the same form. The off-diagonal peaks are labeled $N_{\mathrm{cf}}(t)$ and $N_{\mathrm{fc}}(t)$, indicating that a species began as a complex and ended free or vice versa, respectively

$$N_{cc}(t) = \frac{4}{9} e^{-\alpha T_w}\{\cosh(\beta T_w) - \gamma \sinh(\beta T_w)\} + \frac{5}{9} e^{-\phi T_w}\{\cosh(\varphi T_w) - \theta \sinh(\varphi T_w)\}$$

$$N_{ff}(t) = \frac{4}{9} e^{-\alpha T_w}\{\cosh(\beta T_w) + \gamma \sinh(\beta T_w)\} + \frac{5}{9} e^{-\phi T_w}\{\cosh(\varphi T_w) + \theta \sinh(\varphi T_w)\}$$

$$N_{cf}(t) = N_{fc}(t) = \frac{4}{9}\frac{k_{cf}}{\beta} e^{-\alpha T_w} \sinh(\beta T_w) + \frac{5}{9}\frac{k_{cf}}{\varphi} e^{-\phi T_w} \sinh(\varphi T_w) \quad (11)$$

The definitions of α, β, γ, ϕ, φ, and θ are given in the appendix.

The solutions of eq 10 for $\langle N_f(t) f_f(\theta,t)\rangle$ are composed of contributions from both $N_f(0)$ and $N_c(0)$. The former represents the effective number of oscillating dipoles with $\omega_m = \omega_f$ (vibrational echo emission) that were "frequency-labeled" during the first coherence period as $\omega_\tau = \omega_f$ (frequency of the first interaction). So the contribution from $N_f(0)$ describes the diagonal peak because $\omega_\tau = \omega_f$ and $\omega_m = \omega_f$; the frequency of the first interaction is the same as the frequency of the third interaction and, therefore, vibrational echo emission. The second contribution to $\langle N_f(t) f_f(\theta,t)\rangle$, from $N_c(0)$, involves complexes frequency-labeled by the first interaction with $\omega_\tau = \omega_c$ followed by the third interaction and echo emission at $\omega_m = \omega_f$. This is off-diagonal, corresponding to the dissociation of complexes because the initial interaction is at ω_c, but the final interaction and echo emission is at ω_f. The same considerations apply to $\langle N_c(t) f_c(\theta,t)\rangle$.

The contributions to the diagonal peaks $N_{cc}(t)$ and $N_{ff}(t)$ have two physically different origins. One contribution is from molecules staying in the initial state during the population period without exchange. This subensemble produces an echo signal that is identical to that which would arise from a system with a single species and, therefore, no possibility of chemical exchange. This subensemble can be represented using the response functions for a single oscillator. The other subensemble consists of molecules that undergo an even number of exchanges. For example, a molecule can start in the free form and end in the free form after two exchanges. As a result, such a molecule spends time in the complex form with vibrational lifetime and orientational relaxation rate of the complex form. This type of behavior is included in the kinetic equation and does not require additional treatment.

However, dephasing, described in terms of the response functions given below, is different for the two cases (no exchange versus exchange) even if the echo signals result in a peak at the same position in the 2D spectrum because the two cases involve different quantum pathways. These two cases are described using the Feynman diagrams shown in Figure 2. The contributions from the two cases can be separated using the solutions to the kinetic equations given in eq 11. Consider the effective population N_{ff}. The treatment is identical for N_{cc}. First, N_{ff} without exchange can be calculated by inserting exchange rate as 0, $N_{ff}(t;k_{cf} = 0)$. Then the effective population with exchange, $N_{ff}(t;k_{cf})$, which includes all molecules regardless of whether they happen to exchange or not, is obtained. The difference between these two effective populations gives the population that undergoes multiple exchanges

$$N_{ff}^{ex}(t) = N_{ff}(t;k_{fc} = 0) - N_{ff}(t;k_{fc}) \quad (12)$$

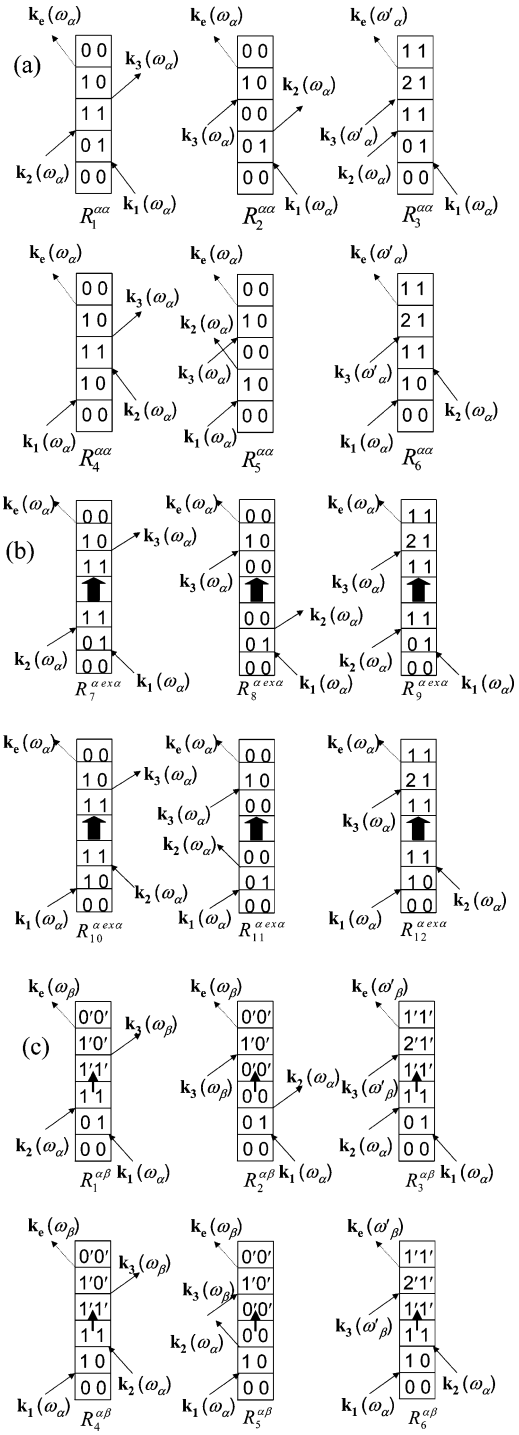

Figure 2. (a) Feynman diagrams corresponding to the first set of response functions. (b) Feynman diagrams corresponding to the second set of response functions. (c) Feynman diagrams corresponding to the third set of response functions.

As a result, the effective population that stays as a free molecule for the entire population period is

$$N_{ff}^{s}(t) = N_{ff}(t;k_c) - N_{ff}^{ex}(t) \quad (13)$$

The effective populations that undergo multiple exchanges, $N_{ff}^{ex}(t)$, and no exchanges, $N_{ff}^{s}(t)$, contribute differently to the total 2D IR spectrum, and these differences are included in the response functions derived in the following section.

B. Response Functions with Exchange. The following response functions were derived using a two-species model.

Kwac et al. obtained response functions for a two-species model.[41] However, the influence of orientational relaxation and lifetimes of the species were not included in the treatment. As discussed with the introduction of the dynamic partition model, for the 2D IR spectroscopic observables, the exchange process and the relaxation processes are coupled. To address this coupling during T_w, the relaxation functions $\Gamma(t_3,T_w,t_1)$ were modified to include exchange. A large number of parameters were included into the calculations. It was possible to measure many of the parameters independently, so that only the exchange rate and the FFCFs were varied to fit the data. The Feynman diagrams for nonlinear response functions are given in Figure 2.

Through the use of the two-species model, the linear response function, $R(t)$, can also be obtained, and they can be expressed as the sum of two terms, one for each species. This model can be generalized to more than two species.

$$R(t) = x_f R_f(t) + x_c R_c(t) \tag{14}$$

Here, x_f and x_c represent free and complex forms' relative populations in the ground state. The x_i can be determined from the analysis of IR spectra as described below. Through the use of the cumulant expansion, the linear response function for each species can be expressed as

$$R_\alpha(t) = |\mu_{0,\alpha}|^2 \, e^{-i\langle\omega_{0,\alpha}\rangle t} \exp\left[-g_{\alpha\alpha}(t) - \frac{1}{2T_1{}^\alpha}t\right] \tag{15}$$

where $\mu_{0,\alpha}$is the transition dipole of the α form, $\langle\omega_{0,\alpha}\rangle$ is the ensemble average 0−1 transition frequency of the α form, and $T_1{}^\alpha$ is the vibrational lifetime of the α form. The line shape function $g_{\alpha\alpha}(t)$ is defined as

$$g_{\alpha\alpha}(t) = \int_0^t d\tau_2 \int_0^{\tau_2} d\tau_1 \, \langle\delta\omega_{\alpha,0}(\tau_1)\delta\omega_{\alpha,0}(0)\rangle \tag{16}$$

where $\langle\delta\omega_{\alpha,0}(\tau_1)\delta\omega_{\alpha,0}(0)\rangle$ is the FFCF.

The analytical expressions for the nonlinear third-order response function use the standard approach and approximations, that is, the Franck−Condon approximation and the cumulant expansion, which apply well to the narrow Gaussian absorption bands.[51] The response functions are composed of two parts, the dephasing functions and the relaxation functions. The dephasing portion describes the time-dependent broadening of the dynamic lines. The relaxation function describes the time-dependent probability of an oscillator contributing to the signal following initial excitation. It can include both a lifetime and an orientational relaxation term as a multiplicative factor for the response function. However, as described above, this is an inadequate method for the problem with exchange. This approach can be used during the coherence periods, but the relaxation function during T_w must be replaced by the solution of the dynamic partition model given in eq 11. The dynamic partition model brings chemical exchange, orientational relaxation, and vibrational relaxation into the calculation in a proper manner that accounts for the differences in lifetimes and orientational relaxation rates of the two species.

For a single line or for two species with no exchange, the degree of frequency correlation between the first coherence period and the final coherence period is determined by the interaction between the oscillator and the bath. Such a correlation still applies to oscillators that do not undergo exchange in a system where exchange is occurring. In the treatment presented here, *we assume that chemical exchange destroys all frequency correlation*. That is, after exchange, an oscillator can assume any frequency in the spectral line with a probability that is only determined by the line shape. There is no memory of the oscillator's location in the spectral line of the species from which it originated. In the systems considered here, a complex and a free species are undergoing chemical exchange. For example, the phenol−benzene complex becomes free phenol in a benzene/CCl_4 mixed solvent. There is an abrupt change in the potential surface, and the surrounding solvent structure must also change. There is little likelihood of correlation. A lack of correlation may also apply to other types of exchange problems, such as isomerization or proton and electron transfer, because of the substantial changes in the nature of the species and the response of the solvent. Nonzero cross correlation is possible in, for example, a hydrogen-bonding system, where the changes in local structure may be small at least on some time scales.[25,44,52]

The assumption of no frequency correlation following chemical exchange means $\langle\delta\omega_\alpha(t)\delta\omega_\beta(0)\rangle = 0$, where α and β represent different species, that is, complex or free. As a result, the line shape of the off-diagonal peaks becomes the product of the linear line shape of the free and complex forms. The lack of frequency correlation following chemical exchange also affects the diagonal peaks because some fraction of the diagonal peaks' signals comes from species that have undergone an even number of exchanges during the T_w period. As a result, part of a diagonal peak's signal will consist of the free induction decay of that species. However, another portion of the signal from oscillators that have not undergone any exchange will have a contribution to the dynamic line shape determined by the coupling to the bath, which is expressed through the FFCF. All of the Feynman diagrams, including all pathways for diagonal peaks, are presented in Figure 2.

The third-order response function for each pathway can be derived analytically. The subscripts SE, GB, and TA in the relaxation functions $\Gamma(t_3,T_w,t_1)$ indicate stimulated emission, ground-state bleaching, and transient absorption, respectively. In the following, $\mu_{0,\alpha}$ and $\mu_{\alpha,2\alpha}$ are the transition dipole matrix elements for the 0−1 and the 1−2 vibrational transitions of the α species. $\Delta_{\alpha,\alpha}$ is the vibrational anharmonicity of the α species. $\omega_{0,\alpha}$ is the center frequency of the 0−1 vibrational transition of the α species.

The first set of response functions (Figure 2a) are for the portion of the diagonal peaks that arise because a subensemble of a species undergoes no exchange, C → {C} → C. These can be expressed as

$$R_1^{\alpha\alpha}(t_3,T_w,t_1) = |\mu_{0,\alpha}|^4 \, e^{-i\langle\omega_{0,\alpha}\rangle(-t_1+t_3)}\Gamma_{SE}^{\alpha\alpha}(t_3,T_w,t_1) \times \exp[-g_{\alpha\alpha}^*(t_1) + g_{\alpha\alpha}^*(T_w) - g_{\alpha\alpha}(t_3) - g_{\alpha\alpha}^*(t_1+T_w) - g_{\alpha\alpha}^*(T_w+t_3) + g_{\alpha\alpha}^*(t_1+T_w+t_3)]$$

$$R_2^{\alpha\alpha}(t_3,T_w,t_1) = |\mu_{0,\alpha}|^4 \, e^{-i\langle\omega_{0,\alpha}\rangle}(-t_1+t_3)\Gamma_{GB}^{\alpha\alpha}(t_3,T_w,t_1) \times \exp[-g_{\alpha\alpha}^*(t_1) + g_{\alpha\alpha}(T_w) - g_{\alpha\alpha}^*(t_3) - g_{\alpha\alpha}^*(t_1+T_w) - g_{\alpha\alpha}(T_w+t_3) + g_{\alpha\alpha}^*(t_1+T_w+t_3)]$$

$$R_3^{\alpha\alpha}(t_3,T_w,t_1) = -|\mu_{0,\alpha}|^2|\mu_{\alpha,2\alpha}|^2 \, e^{-i[\langle\omega_{0,\alpha}\rangle(-t_1+t_3)-\Delta_{\alpha,\alpha}t_3]}\Gamma_{TA}^{\alpha\alpha}(t_3,T_w,t_1) \times \exp[-g_{\alpha\alpha}^*(t_1) + g_{\alpha\alpha}(T_w) - g_{\alpha\alpha}(t_3) - g_{\alpha\alpha}(t_1+T_w) - g_{\alpha\alpha}(T_w+t_3) + g_{\alpha\alpha}(t_1+T_w+t_3)]$$

$$R_4^{\alpha\alpha}(t_3,T_w,t_1) = |\mu_{0,\alpha}|^4 \, e^{-i\langle\omega_{0,\alpha}\rangle(-t_1+t_3)}\Gamma_{SE}^{\alpha\alpha}(t_3,T_w,t_1) \times \exp[-g_{\alpha\alpha}(t_1) - g_{\alpha\alpha}(T_w) - g_{\alpha\alpha}(t_3) + g_{\alpha\alpha}(t_1+T_w) + g_{\alpha\alpha}(T_w+t_3) - g_{\alpha\alpha}(t_1+T_w+t_3)]$$

$$R_5^{\alpha\alpha}(t_3,T_w,t_1) = |\mu_{0,\alpha}|^4\, e^{-i\langle\omega_{0,\alpha}\rangle(-t_1+t_3)}\Gamma_{GB}^{\alpha\alpha}(t_3,T_w,t_1) \times \exp[-g_{\alpha\alpha}(t_1) - g^*_{\alpha\alpha}(T_w) - g^*_{\alpha\alpha}(t_3) + g_{\alpha\alpha}(t_1+T_w) + g^*_{\alpha\alpha}(T_w+t_3) - g_{\alpha\alpha}(t_1+T_w+t_3)]$$

$$R_6^{\alpha\alpha}(t_3,T_w,t_1) = -|\mu_{0,\alpha}|^2|\mu_{\alpha,2\alpha}|^2\, e^{-i[\langle\omega_{0,\alpha}\rangle(-t_1+t_3)-\Delta_{\alpha,\alpha}t_3]}\Gamma_{TA}^{\alpha\alpha}(t_3,T_w,t_1) \times \exp[-g_{\alpha\alpha}(t_1) - g^*_{\alpha\alpha}(T_w) - g_{\alpha\alpha}(t_3) + g^*_{\alpha\alpha}(t_1+T_w) + g^*_{\alpha\alpha}(T_w+t_3) - g^*_{\alpha\alpha}(t_1+T_w+t_3)]$$

$$\Gamma_{SE}^{\alpha\alpha}(t_3,T_w,t_1) = \exp\left[-2D_\alpha t_1 - 2D_\alpha t_3 - \frac{1}{2T_1{}^\alpha}t_1 - \frac{1}{2T_1{}^\alpha}t_3\right]N^s_{\alpha\alpha}(T_w)$$

$$\Gamma_{GB}^{\alpha\alpha}(t_3,T_w,t_1) = \exp\left[-2D_\alpha t_1 - 2D_\alpha t_3 - \frac{1}{2T_1{}^\alpha}t_1 - \frac{1}{2T_1{}^\alpha}t_3\right]N^s_{\alpha\alpha}(T_w)$$

$$\Gamma_{TA}^{\alpha\alpha}(t_3,T_w,t_1) = \exp\left[-2D_\alpha t_1 - 2D_\alpha t_3 - \frac{1}{2T_1{}^\alpha}t_1 - \frac{1}{T_1{}^\alpha}t_3\right]N^s_{\alpha\alpha}(T_w)$$

As discussed above, these response functions show the same behavior as a species without exchange.

The second set of response functions (Figure 2b) for the diagonal peaks describes the subensemble of a species that undergoes an even number of exchanges, C → {C → F → C} → C. As discussed above, these exchanges destroy all frequency correlation. So the final expressions for these pathways are

$$R_7^{\alpha\alpha}(t_3,T_w,t_1) = |\mu_{0,\alpha}|^4\, e^{-i\langle\omega_{0,\alpha}\rangle(-t_1+t_3)}\Gamma_{SE}^{\alpha ex\alpha}(t_3,T_w,t_1) \times \exp[-g^*_{\alpha\alpha}(t_1) - g_\alpha\alpha(t_3)]$$

$$R_8^{\alpha\alpha}(t_3,T_w,t_1) = |\mu_{0,\alpha}|^4\, e^{-i\langle\omega_{0,\alpha}\rangle(-t_1+t_3)}\Gamma_{GB}^{\alpha ex\alpha}(t_3,T_w,t_1) \times \exp[-g^*_{\alpha\alpha}(t_1) - g^*_{\alpha\alpha}(t_3)]$$

$$R_9^{\alpha\alpha}(t_3,T_w,t_1) = -|\mu_{0,\alpha}|^2|\mu_{\alpha,2\alpha}|^2\, e^{-i[\langle\omega_{0,\alpha}\rangle(-t_1+t_3)-\Delta_{\alpha,\alpha}t_3]}\Gamma_{TA}^{\alpha ex\alpha}(t_3,T_w,t_1) \times \exp[-g^*_{\alpha\alpha}(t_1) - g_{\alpha\alpha}(t_3)]$$

$$R_{10}^{\alpha\alpha}(t_3,T_w,t_1) = |\mu_{0,\alpha}|^4\, e^{-i\langle\omega_{0,\alpha}\rangle(-t_1+t_3)}\Gamma_{SE}^{\alpha ex\alpha}(t_3,T_w,t_1) \times \exp[-g_\alpha\alpha(t_1) - g^*_{\alpha\alpha}(t_3)]$$

$$R_{11}^{\alpha\alpha}(t_3,T_w,t_1) = |\mu_{0,\alpha}|^4\, e^{-i\langle\omega_{0,\alpha}\rangle(-t_1+t_3)}\Gamma_{GB}^{\alpha ex\alpha}(t_3,T_w,t_1) \times \exp[-g_{\alpha\alpha}(t_1) - g^*_{\alpha\alpha}(t_3)]$$

$$R_{12}^{\alpha\alpha}(t_3,T_w,t_1) = -|\mu_{0,\alpha}|^2|\mu_{\alpha,2\alpha}|^2\, e^{-i\langle\omega_{0,\alpha}\rangle(-t_1+t_3)-\Delta_{\alpha,\alpha}t_3}\Gamma_{TA}^{\alpha ex\alpha}(t_3,T_w,t_1) \times \exp[-g_{\alpha\alpha}(t_1) - g_{\alpha\alpha}(t_3)]$$

$$\Gamma_{SE}^{\alpha ex\alpha}(t_3,T_w,t_1) = \exp\left[-2D_\alpha t_1 - 2D_\alpha t_3 - \frac{1}{2T_1{}^\alpha}t_1 - \frac{1}{2T_1{}^\alpha}t_3\right]N^{ex}_{\alpha\alpha}(T_w)$$

$$\Gamma_{GB}^{\alpha ex\alpha}(t_3,T_w,t_1) = \exp\left[-2D_\alpha t_1 - 2D_\alpha t_3 - \frac{1}{2T_1{}^\alpha}t_1 - \frac{1}{2T_1{}^\alpha}t_3\right]N^{ex}_{\alpha\alpha}(T_w)$$

$$\Gamma_{TA}^{\alpha ex\alpha}(t_3,T_w,t_1) = \exp\left[-2D_\alpha t_1 - 2D_\alpha t_3 - \frac{1}{2T_1{}^\alpha}t_1 - \frac{1}{T_1{}^\alpha}t_3\right]N^{ex}_{\alpha\alpha}(T_w)$$

The dephasing functions for these pathways show no dependence on T_w because of the assumption of no frequency correlation following exchange. So the contribution to the line shape from these pathways has no information for spectral diffusion dynamics. There is a dependence on T_w contained in the effective population term, $N^{ex}_{\alpha\alpha}(T_w)$. $N^{ex}_{\alpha\alpha}(T_w)$ determines the contribution of the fully broadened line shape to the dynamic line shape of the diagonal peaks. Without the separation into the first set of response functions and the second set of response functions for diagonal peaks, an observed fast broadening of the diagonal peaks caused by exchange could be misinterpreted as a result of spectral diffusion.

The third set of response functions (Figure 2c) for the off-diagonal peaks from a subensemble of a species that undergoes at least one exchange or any odd number of exchanges, C → {C → F} → F. All contributions to the off-diagonal peaks include at least one exchange, which destroys all frequency correlation. For this reason, the line shape of the off-diagonal peaks is a product of the linear line shapes of the two species.

$$R_1^{\alpha\beta}(t_3,T_w,t_1) = |\mu_{0,\alpha}|^2|\mu_{0,\beta}|^2\, e^{i\langle\omega_{0,\alpha}\rangle t_1 - i\langle\omega_{0,\beta}\rangle t_3}\Gamma_{SE}^{\alpha\beta}(t_3,T_w,t_1) \times \exp[-g^*_{\alpha\alpha}(t_1) - g_{\beta\beta}(t_3)]$$

$$R_2^{\alpha\beta}(t_3,T_w,t_1) = |\mu_{0,\alpha}|^2|\mu_{0,\beta}|^2\, e^{i\langle\omega_{0,\alpha}\rangle t_1 - i\langle\omega_{0,\beta}\rangle t_3}\Gamma_{GB}^{\alpha\beta}(t_3,T_w,t_1) \times \exp[-g^*_{\alpha\alpha}(t_1) - g^*_{\beta\beta}(t_3)]$$

$$R_3^{\alpha\beta}(t_3,T_w,t_1) = -|\mu_{0,\alpha}|^2|\mu_{\beta,2\beta}|^2\, e^{i\langle\omega_{0,\alpha}\rangle t_1 - i[\langle\omega_{0,\beta}\rangle-\Delta_{\beta,\beta}]t_3}\Gamma_{TA}^{\alpha\beta}(t_3,T_w,t_1) \times \exp[-g^*_{\alpha\alpha}(t_1) - g_{\beta\beta}(t_3)]$$

$$R_4^{\alpha\beta}(t_3,T_w,t_1) = |\mu_{0,\alpha}|^2|\mu_{0,\beta}|^2\, e^{-i\langle\omega_{0,\alpha}\rangle t_1 - i\langle\omega_{0,\beta}\rangle t_3}\Gamma_{SE}^{\alpha\beta}(t_3,T_w,t_1) \times \exp[-g_{\alpha\alpha}(t_1) - g_{\beta\beta}(t_3)]$$

$$R_5^{\alpha\beta}(t_3,T_w,t_1) = |\mu_{0,\alpha}|^2|\mu_{0,\beta}|^2\, e^{-i\langle\omega_{0,\alpha}\rangle t_1 - i\langle\omega_{0,\beta}\rangle t_3}\Gamma_{GB}^{\alpha\beta}(t_3,T_w,t_1) \times \exp[-g_\alpha\alpha(t_1) - g^*_{\beta\beta}(t_3)]$$

$$R_6^{\alpha\beta}(t_3,T_w,t_1) = -|\mu_{0,\alpha}|^2|\mu_{\beta,2\beta}|^2\, e^{-i\langle\omega_{0,\alpha}\rangle t_1 - i[\langle\omega_{0,\beta}\rangle-\Delta_{\beta,\beta}]t_3}\Gamma_{TA}^{\alpha\beta}(t_3,T_w,t_1) \times \exp[-g_{\alpha\alpha}(t_1) - g_{\beta\beta}(t_3)]$$

$$\Gamma_{SE}^{\alpha\beta}(t_3,T_w,t_1) = \exp\left[-2D_\alpha t_1 - 2D_\beta t_3 - \frac{1}{2T_1{}^\alpha}t_1 - \frac{1}{2T_1{}^\beta}t_3\right]N_{\alpha\beta}(T_w)$$

$$\Gamma_{GB}^{\alpha\beta}(t_3,T_w,t_1) = \exp\left[-2D_\alpha t_1 - 2D_\beta t_3 - \frac{1}{2T_1{}^\alpha}t_1 - \frac{1}{2T_1{}^\beta}t_3\right]N_{\alpha\beta}(T_w)$$

$$\Gamma_{TA}^{\alpha\beta}(t_3,T_w,t_1) = \exp\left[-2D_\alpha t_1 - 2D_\beta t_3 - \frac{1}{2T_1{}^\alpha}t_1 - \frac{1}{T_1{}^\beta}t_3\right]N_{\alpha\beta}(T_w)$$

As discussed in the Experimental Section, rephasing (R) and nonrephasing (NR) signals are collected separately and added after Fourier transformation to eliminate a substantial portion of the dispersive contribution to the signal.[34] To emulate the experimental signal, calculation of the data mimicked he experimental procedure. The total rephrasing response function $R_R(t_1,T_w,t_3)$ and nonrephrasing response function $R_{NR}(t_1,T_w,t_3)$ are defined as

$$R_{\mathrm{R}}(t_1,T_{\mathrm{w}},t_3) = \sum_{i=1}^{3}\sum_{\alpha,\beta}(R_i^{\alpha\alpha}(t_1,T_{\mathrm{w}},t_3) + R_{6+i}^{\alpha\alpha}(t_1,T_{\mathrm{w}},t_3) + R_i^{\alpha\beta}(t_1,T_{\mathrm{w}},t_3)) \quad (17)$$

$$R_{\mathrm{NR}}(t_1,T_{\mathrm{w}},t_3) = \sum_{i=4}^{6}\sum_{\alpha,\beta}(R_i^{\alpha}\alpha(t_1,T_{\mathrm{w}},t_3) + R_{6+i}^{\alpha\alpha}(t_1,T_{\mathrm{w}},t_3) + R_i^{\alpha\beta}(t_1,T_{\mathrm{w}},t_3)) \quad (18)$$

The final 2D vibrational echo spectrum is

$$S_{2D}(\omega_\tau,\omega_{\mathrm{m}},T_{\mathrm{w}}) \propto \{\mathrm{Re}\}[\tilde{R}_{\mathrm{R}}(\omega_\tau,\omega_{\mathrm{m}},T_{\mathrm{w}}) + \tilde{R}_{\mathrm{NR}}(\omega_\tau,\omega_{\mathrm{m}},T_{\mathrm{w}})] \quad (19)$$

where $\tilde{R}_{\mathrm{R}}$ and $\tilde{R}_{\mathrm{NR}}$ are defined as

$$\tilde{R}_{\mathrm{R}}(\omega_\tau,\omega_{\mathrm{m}},T_{\mathrm{w}}) = \int_0^\infty \mathrm{d}t_1 \int_0^\infty \mathrm{d}t_3 \exp(\mathrm{i}\omega_{\mathrm{m}}t_3 - \mathrm{i}\omega_\tau t_1)R_{\mathrm{R}}(t_1,T_{\mathrm{w}},t_3) \quad (20)$$

$$\tilde{R}_{\mathrm{NR}}(\omega_\tau,\omega_{\mathrm{m}},T_{\mathrm{w}}) = \int_0^\infty \mathrm{d}t_1 \int_0^\infty \mathrm{d}t_3 \exp(\mathrm{i}\omega_{\mathrm{m}}t_3 + \mathrm{i}\omega_\tau t_1)R_{\mathrm{NR}}(t_1,T_{\mathrm{w}},t_3) \quad (21)$$

V. Data Calculations Using the Response Functions with Exchange

The experimental 2D spectra are fit using the response functions with the exchange rate and FFCF as adjustable parameters. The entire region of 2D spectra including the 0−1 and 1−2 portions were calculated and compared to the experiments. Necessary input parameters, that is, the ratio of the transition dipole matrix elements for the complex and free form, the steady-state ratio of the complex and free populations (equilibrium constant), the vibrational lifetimes, and the orientational relaxation rates, were determined from linear-IR and pump−probe experiments.

For each of the three complex systems, phenol with benzene, *p*-xylene, and bromobenzene, the same procedures were employed. Each system contained phenol as the solute and one of the three complex partners as a mixed solvent with CCl_4. The methodology is discussed here for the phenol. All of the systems were treated in the same manner.

Pump−probe measurements were performed on three different samples, phenol in the mixed solvent (benzene/CCl_4), phenol in pure CCl_4, and phenol in pure benzene (Table 1). The pump−probe spectrum of phenol in benzene/CCl_4 is used for obtaining the properly "phased" 2D vibration echo spectra by employing the projection slice theorem.[35,36] The measurements of the pump−probe decays on phenol in the two pure solvents were used to obtained the vibrational lifetimes and orientational relaxation rates (Table 1). With benzene as the solvent, the equilibrium is shifted to virtually all complex, and the pump−probe experiment gives the vibrational lifetime of the complex. In CCl_4 there is no complex, and the lifetime of the free species is obtained. The mixed solvent may have a small effect on the lifetimes, but the calculation is not highly sensitive to small uncertainties in the lifetimes. The orientational relaxation obtained from polarized pump−probe experiments on the two pure solvents gives the orientational relaxation rates for the complex and the free form. These were corrected for the change in viscosity in going to the mixed solvent using the Debye−Stokes−Einstein equation, $\tau_{\mathrm{r}} = V_{\mathrm{eff}}\eta/k_{\mathrm{B}}T$, where V_{eff} is the effective volume, η is the viscosity, k_{B} is Boltzmann's constant, and T is the temperature. The viscosity of each pure and mixed solvent was measured at the experimental temperature (24 °C). The values used in the response function calculations are given in Table 2. These experimentally determined lifetimes and orientational relaxation rates were used without adjustment in the response function calculations. The transition dipole matrix elements for the two species were determined by measuring the absorption spectra in the two pure solvents for a known concentration of phenol. Once the ratio of the transition dipole matrix elements was known (Table 2), it was used to analyze the spectrum in the mixed solvent in which the complex peak and the free peak have approximately the same amplitudes (Figure 3a). The spectra were fit, and using the transition dipole matrix element ratio, the equilibrium constant and therefore the ratio of the concentrations of the two species were determined (Table 2).

TABLE 1: Vibrational Lifetimes (T_1) and Orientational Relaxation Time Constants (τ_r) of Phenol in Various Pure Solvents Measured with the Pump−Probe Experiment[a]

solvent	T_1 (ps)	τ_r (ps)
CCl_4	12.5	2.9
benzene	10	3.4
p-xylene	9.2	5.0
bromobenzene	10	3.1

[a] In CCl_4, phenol is not complexed. In the other three solvents, it is a complex with a solvent molecule. The τ_{r} values used in the analysis were corrected for the changes in viscosity from the pure solvents to the mixed solvents. See Table 2 for values used in calculations.

TABLE 2: Constants Used in the Response Function Calculations[a]

solvent	phenol species	T_1 (ps)	τ_{r} (ps)	μ_c/μ_f	[complex]/[free]
p-xylene/CCl_4	free	12.5	2.9	1.6	0.83
	complex	9.2	4.3		
benzene/CCl_4	free	12.5	2.9	1.5	0.8
	complex	10	3.4		
bromobenzene/CCl_4	free	12.5	2.9	1.23	1.32
	complex	10	3.1		

[a] The orientational relaxation times were corrected from the measured values (Table 1) for the changes in viscosity in the mixed solvents.

To determine the exchange rate and the FFCF, the entire 2D vibrational echo spectrum was fit as follows. It is important to note that the exchange rate and the FFCF are relatively independent. The exchange rate determines the growth of the off-diagonal peaks and contributes to the decay of the diagonal peaks. The FFCF determines the time-dependent shape of the diagonal peaks. However, the rate of exchange also has an influence on the shape of the diagonal peaks, but the FFCF has no influence on the growth of the off-diagonal peaks. Various functional forms of the FFCF were tested, and it was determined that a biexponential function was sufficient to reproduce the data.

$$\langle\delta\omega(t)\delta\omega(0)\rangle = \Delta_0^{\,2}\exp(-t/\tau_0) + \Delta_1^{\,2}\exp(-t/\tau_1) \quad (22)$$

The biexponential FFCF includes a slow component (>1 ps) and a fast component (<1ps). These constraints were implemented in the fitting routine with the amplitudes and decay constants allowed to float. First, the 2D spectrum for each T_{w} point was fit separately. The parameters were iterated to minimize the residuals. Two-dimensional matrices that contain the intensity of each (ω_τ,ω_{m}) point from the experiment and the calculation are compared. A nonlinear multivariable fitting

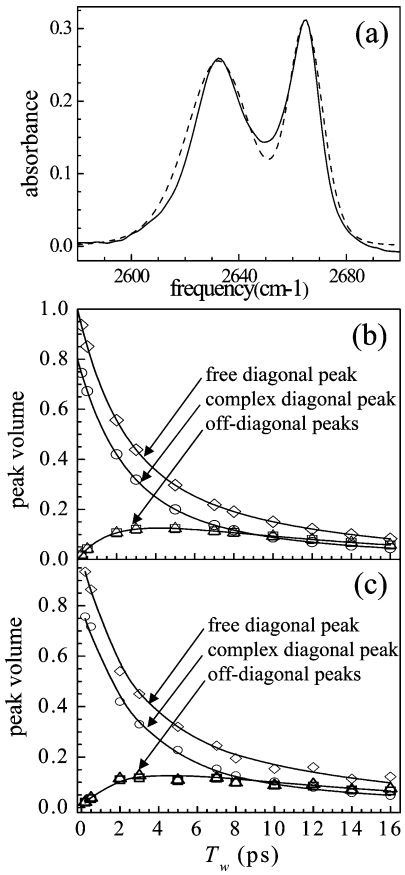

Figure 3. (a) Spectrum of the hydroxyl stretch of phenol-OD in the benzene/CCl_4 mixed solvent (solid curve) and the calculated spectrum (dashed curve). The high-frequency peak is the free phenol, and the low-frequency peak is the phenol−benzene complex. The calculated spectrum used the FFCF obtained by fitting the 2D vibrational echo spectra (Figure 1, bottom). (b) The points are peak volumes obtained from the response function calculation. The solid curves were obtained from fits using the peak volume method discussed in section VI. (c) The points are peak volumes obtained by fitting the 2D vibrational echo spectrum (Figure 1, top) using the peak volume method (section VI). The solid curves are fits to the peak volumes.

routine with a direct line search algorithm is used. To avoid false minima, many different initial conditions were used in the fitting program. As a check on the resulting parameters, the linear spectrum was calculated using the FFCF. This procedure was repeated for every data set with different T_w points. After optimized parameters for each T_w point were obtained, they were averaged to produce one parameter set. These averaged parameters were then used as the initial parameters for fitting the 2D spectra at all T_w values simultaneously. As a final test of the resulting parameters, the linear absorption line shape was calculated and compared to the data. The resulting complex dissociation times and FFCFs for the three systems studied are presented in the Table 3. The dissociation times are listed because this is the single parameter required to describe the chemical exchange process. The complex and the free form are in equilibrium. Therefore, the rate of complex dissociation is equal to the rate of complex formation, and the rate of complex dissociation can be characterized by the dissociation time.

In the top of Figure 1, data from a few of the T_w points are shown. The calculated 2D spectra for these points are shown in the bottom portion of the figure. Inspection of the two sets of figures shows that the calculation does a good job of reproducing the data. The response function calculations reproduce the experimental spectra including the growth of the off-diagonal peaks and the tilt of the diagonal peaks at short T_w, which disappears as time progresses because of spectral diffusion. (An insufficient number of 2D spectra are shown at short times to see the progression of the spectral diffusion.)

TABLE 3: Frequency−Frequency Correlation Function (FFCF) Parameters (Eq 22) and Complex Dissociation Times, $\tau_d = 1/k_{cf}$, for the Solute−Solvent Systems that Form the Complexes Phenol−*p*-Xylene, Phenol−Benzene, and Phenol−Bromobenzene[a]

complex		Δ_0 (rad/ps)	τ_0 (ps)	Δ_1 (rad/ps)	τ_1 (ps)	τ_d (ps)
phenol−*p*-xylene	free			1.1	2.3	21
	complex	3.0	0.10	1.7	2.4	
phenol−benzene	free			1.3	1.9	8
	complex	2.5	0.44	1.4	1.8	
phenol−bromobenzene	free			1.5	1.1	6
	complex	2.6	0.71	1.2	1.7	

[a] The FFCF parameters are for both the complex and the free phenol.

Figure 3 provides additional insights as to the ability of the calculation to quantitatively reproduce the data. Figure 3a shows the absorption spectrum of the phenol-OD hydroxyl stretch along with the calculated spectrum obtained from the FFCF and eqs 15 and 16 with only a scaling factor as an adjustable parameter. Figure 3b shows calculations of the volumes of each of the four peaks (two diagonal and two off-diagonal) in the 0−1 region of the spectrum. The volumes were obtained by using the portions of the response functions that give rise to each peak individually and then integrating the resulting peak. These are the points in the figure. The calculated points for the two off-diagonal peaks fall on top of each other because the system is in thermal equilibrium. Therefore, the rate of complex formation is equal to the rate of complex dissociation. Tests showing that the systems are in thermal equilibrium have been presented.[1] The curves through the points were obtained previously[1] using the peak volume fitting method, which will be discussed in section VI. The agreement between the response function calculated points and the calculations that do not include spectral diffusion explicitly shows that the use of the more detailed response function method does not distort analysis of the chemical exchange dynamics.

Figures 4 and 5 display data and calculations for the phenol−*p*-xylene system, and Figures 6 and 7 display data and calculations for the phenol−bromobenzene system. The top portions of Figures 4 and 6 show the 2D spectra, and the bottom portions show the calculated 2D spectra. Figures 5a and 7a show the linear absorption spectra and the spectra calculated using the FFCF obtained from fitting the 2D spectra. Figures 5b and 7b show the response function method calculated peak volumes (points) and the curves obtained by using the peak volume fitting method (discussed in section VI). All of the procedures discussed in terms of the phenol−benzene system were applied in an identical manner to the other systems. In all cases the response function calculations do a good job of reproducing the 2D spectra and the linear spectra and agree with the less detailed peak volume method that gives only the chemical exchange dynamics.

The FFCF parameters obtained from the response function fits to the data are given in Table 3. For each solute−solvent system there are two species, the complex and the free phenol. For each system, the complex hydroxyl stretch dephasing is significantly different from the dephasing of the free phenol hydroxyl stretch. Although a biexponential form of the FFCF was used (eq 22), it was found that the fit for the data from the

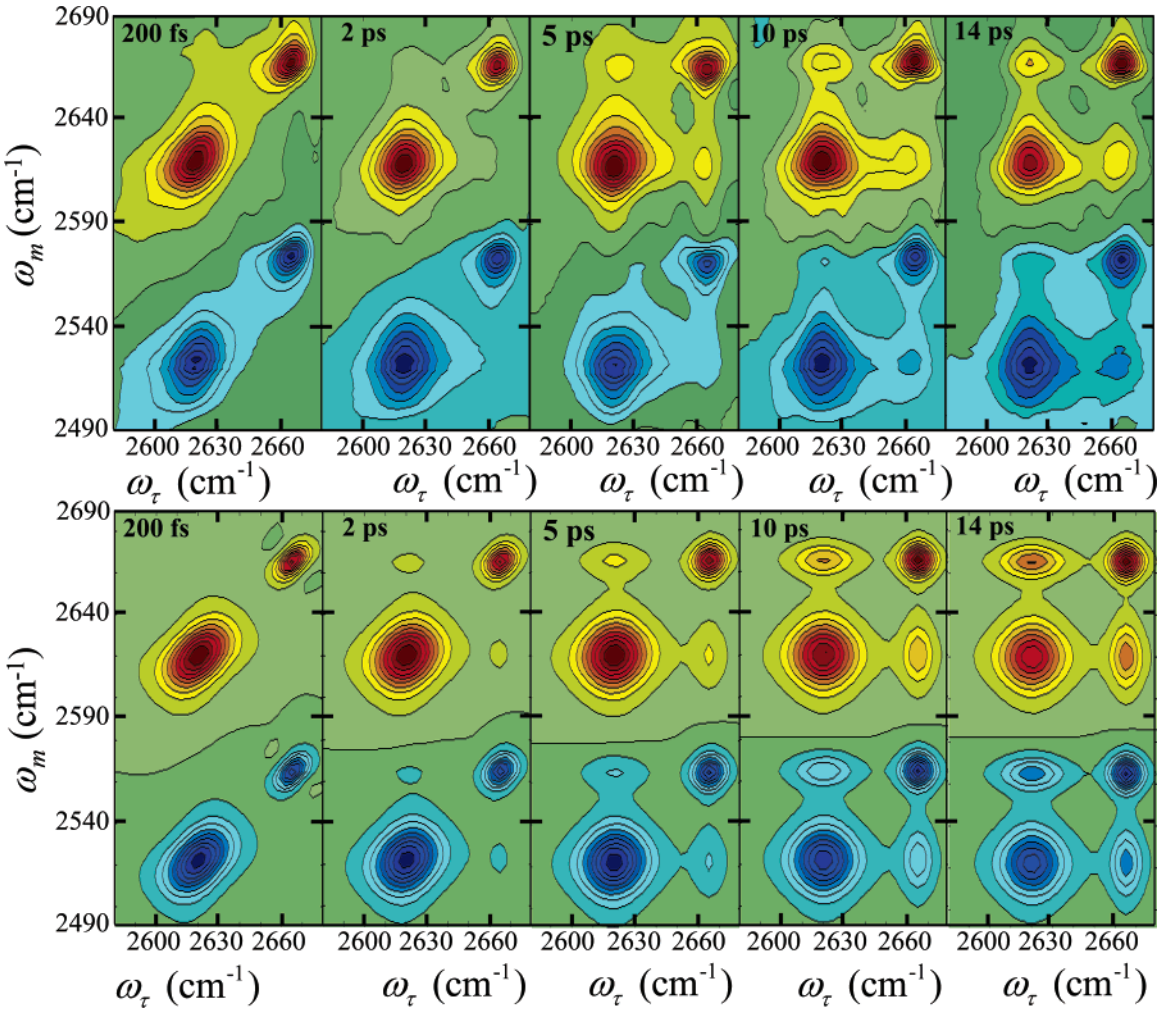

Figure 4. T_w-dependent 2D IR vibrational echo spectra (top) of the hydroxyl stretch of phenol-OD in *p*-xylene/CCl_4 mixed solvents (molar ratios of phenol/*p*-xylene/CCl_4 = 1:21:100). The red peaks (positive) are from the 0−1 vibration transitions, and the blue peaks (negative) are from the 1−2 vibrational transitions. At 200 fs, there are two peaks on the diagonal (red) and two peaks below these (blue) shifted by the anharmonicity. As T_w increases, additional peaks appear due to chemical exchange, that is, dissociation and formation of the phenol−*p*-xylene complex. The bottom portion displays response function calculations of the data.

free species converged to a single exponential. However, the data from the complex could not be fit well with a single-exponential FFCF. (It is important to note that these are single and biexponential FFCFs, both of which give rise to time-dependent observable broadening of the diagonal peaks along the ω_τ axis that is not exponential or biexponential.)

In each of the three systems, Δ_1 and τ_1 in Table 3 are similar for the complex and free forms. This similarity strongly suggests that this component of the FFCF arises from the effect of solvent fluctuation on the hydroxyl stretching frequency. These solvent fluctuations and their influence are not strongly dependent on complexation. However, only the complexed forms have the fast component, that is, Δ_0 and τ_0, which strongly suggests that this component is caused by fluctuation in the actual complex structure. The complex involves a weak π-hydrogen bond between the hydroxyl and the solvent aromatic ring. Electronic structure calculations have shown the structure of the phenol−benzene complex.[1] It would be expected that fluctuation of the complex structure would be a major source of vibrational dephasing.

The dissociation times listed in Table 3 decrease as the solute−solvent complex becomes weaker. In *p*-xylene, the methyl groups donate electron density to the benzene π-system, which results in a stronger complex than that with benzene. In bromobenzene, the bromo group withdraws electron density, producing a weaker complex than that with benzene. These qualitative considerations are born out by measurements of the bond enthalpies, ΔH_0, of the complexes.[1] The ΔH_0 values extracted from van't Hoff plots were −1.21 kcal/mol for the phenol−bromobenzene complex, −1.67 kcal/mol for the phenol−benzene complex, and −2.23 kcal/mol for the phenol−*p*-xylene complex. Thus, as the bond enthalpy increases (stronger bond), the dissociation time τ_d also increases, because the free energy of activation for dissociation ($\Delta G^\ddagger$) would be expected to scale with the bond enthalpies.

It is also interesting to note that the fast component of the FFCF, τ_0, also appears to change with the change in the bond enthalpies. The Δ_0 values are very similar for the three complexes. This similarity means that the ranges of frequencies sampled because of fluctuations in the structures of the complexes are about the same. However, τ_0 becomes faster as the complex bond becomes stronger. The faster decay of this component of the FFCF with increasing bond strength might reflect a higher-frequency intermolecular quasi-vibration associated with the stronger complex.

VI. Comparison to the Peak Volume Only Fitting Method

Through the use of the response functions with the dynamic partition model, very good fits were obtained to the 2D spectra,

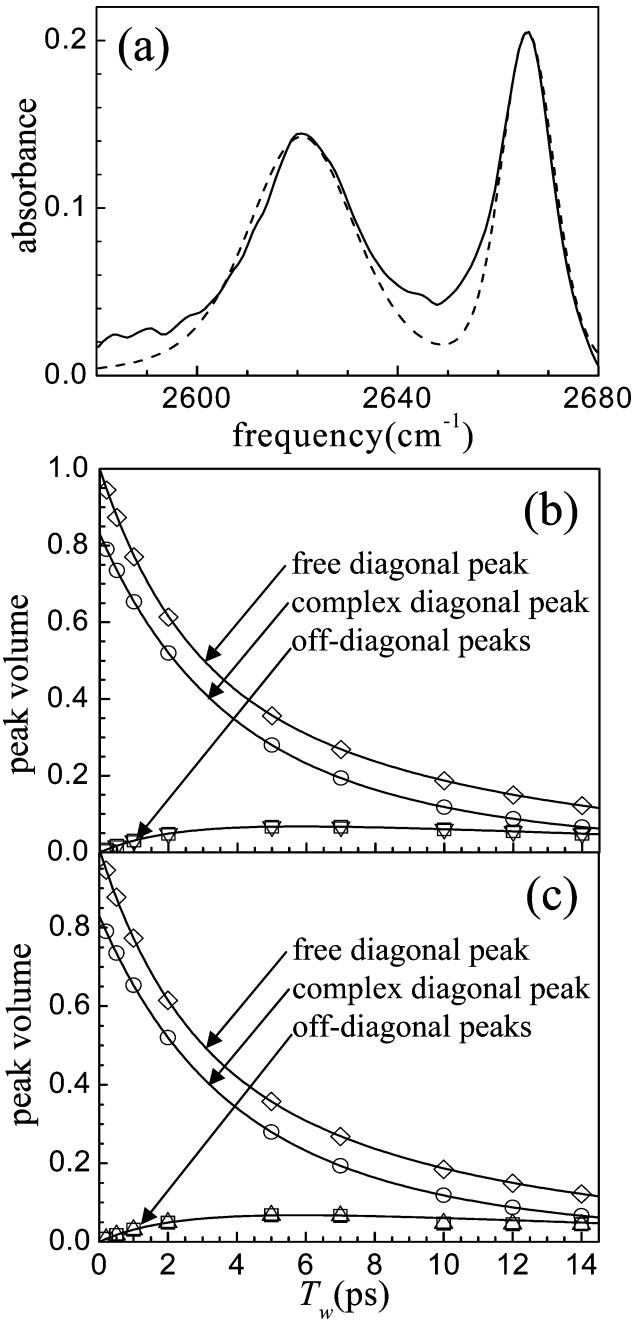

Figure 5. (a) Spectrum of the hydroxyl stretch of phenol-OD in the *p*-xylene/CCl_4 mixed solvent (solid curve) and the calculated spectrum (dashed curve). The high-frequency peak is the free phenol, and the low-frequency peak is the phenol−*p*-xylene complex. The calculated spectrum used the FFCF obtained by fitting the 2D vibrational echo spectra (Figure 4, bottom). (b) The points are peak volumes obtained from the response function calculation. The solid curves were obtained from fits using the peak volume method discussed in section VI. (c) The points are peak volumes obtained by fitting the 2D vibrational echo spectra (Figure 4, top) using the peak volume method (section VI). The solid curves are fits to the peak volumes.

and both the parameters for the FFCFs and the dissociation times were extracted from the data. Previously, a much simpler method was used to obtain the complex dissociation times for both phenol complexes[1] discussed here and complexes involving 2-methoxyphenol with several aromatic solvents.[2] This method provides no information on the spectral diffusion (FFCF) but uses the peak volumes and the dynamic partition model to extract the exchange kinetics. In the absence of any other process, spectral diffusion broadens the 2D peaks along the ω_τ axis. However, the volumes of the peaks are preserved. When exchange, vibrational, and orientational relaxation are occurring in addition to spectral diffusion, the peak amplitudes cannot be used to determine the population kinetics because of the change in shapes of the peaks produced by spectral diffusion. It was proposed that if the peak volumes were fit as a function of T_w, then the influence of spectral diffusion would be swept into the fit, and a detailed treatment, as presented here, was unnecessary to determine the exchange kinetics.[1] It is important to test this volume fitting approach because it is relatively simple to apply to obtain the exchange kinetics.

In the volume fitting method, the volume of each peak in the 2D IR spectrum was determined by fitting the entire 0−1 spectrum (or the full spectrum) composed of overlapping peaks. Each peak was approximated as a "tilted" two-dimensional Gaussian function

$$F(\phi,\omega_1,\omega_2,\sigma(\mathrm{d}),\sigma(\mathrm{a}),A) = \sum_{i=1}^{4} A_i \frac{\exp(-((\cos\phi)(\omega_m-\omega_j)+(\sin\phi)(\omega_\tau-\omega_j))^2)}{2(\sigma_i(\mathrm{d}))^2} \times \frac{\exp(-(-(\sin\phi)(\omega_m-\omega_j)+(\cos\phi)(\omega_\tau-\omega_j))^2)}{2(\sigma_i(\mathrm{a}))^2} \quad (23)$$

This function was used to reproduce the shape of each peak. Here, tilt angle (ϕ), line widths along the diagonal (σ(d)) and antidiagonal (σ(a)), and amplitude (A) are used as parameters for fitting the experimental data and obtaining the volume corresponding to each individual peak.

Each peak volume is corrected by the appropriate products of the transition dipole moments (μ_i^4 for the diagonal peaks and $\mu_i^2\mu_j^2$ for the off-diagonal peaks), and the largest volume peak at the shortest time is normalized to the corresponding solution of eq 11 at that time. All other peaks at any time have a volume relative to this normalized volume. Equations 11 for effective populations, $N_{\alpha\beta}(t)$, are fit to the volumes of the set of peaks at each T_w. As with the response function calculations, the independently measured lifetimes, orientational relaxation rates, transition dipole moment ratio, and the equilibrium population ratio are used as fixed input parameters. The result is that there is a single adjustable parameter, the dissociation time, τ_d. All of the 2D spectra are fit simultaneously with this single parameter.

Figures 3c, 5c, and 7c show the results of using the peak volume fitting method. Ihe identical complex dissociation times are obtained using the full response function calculations or the peak volume method. The curves in Figures 3b, 5b, and 7b are the same curves as those in Figures 3c, 5c, and 7c. In the parts b of the figures, the points were obtained from the response function calculations that fit the full 2D spectra including spectral diffusion. Therefore, if the chemical exchange kinetics are the sole interest, then these can be obtained without the complexity of using the response function approach but with the loss of information from the FFCFs. It is important to point out that to extract the chemical exchange kinetics with the peak volume fitting method quantitatively is still not simple. First, it is necessary to use the dynamic partition model (eqs 11) to account for orientational relaxation rates and vibrational lifetimes in addition to the chemical exchange. To reduce the input parameters, it is necessary to independently measure orientational relaxation rates, lifetimes, the transition dipole ratio, and the equilibrium population ratio. However, with these inputs

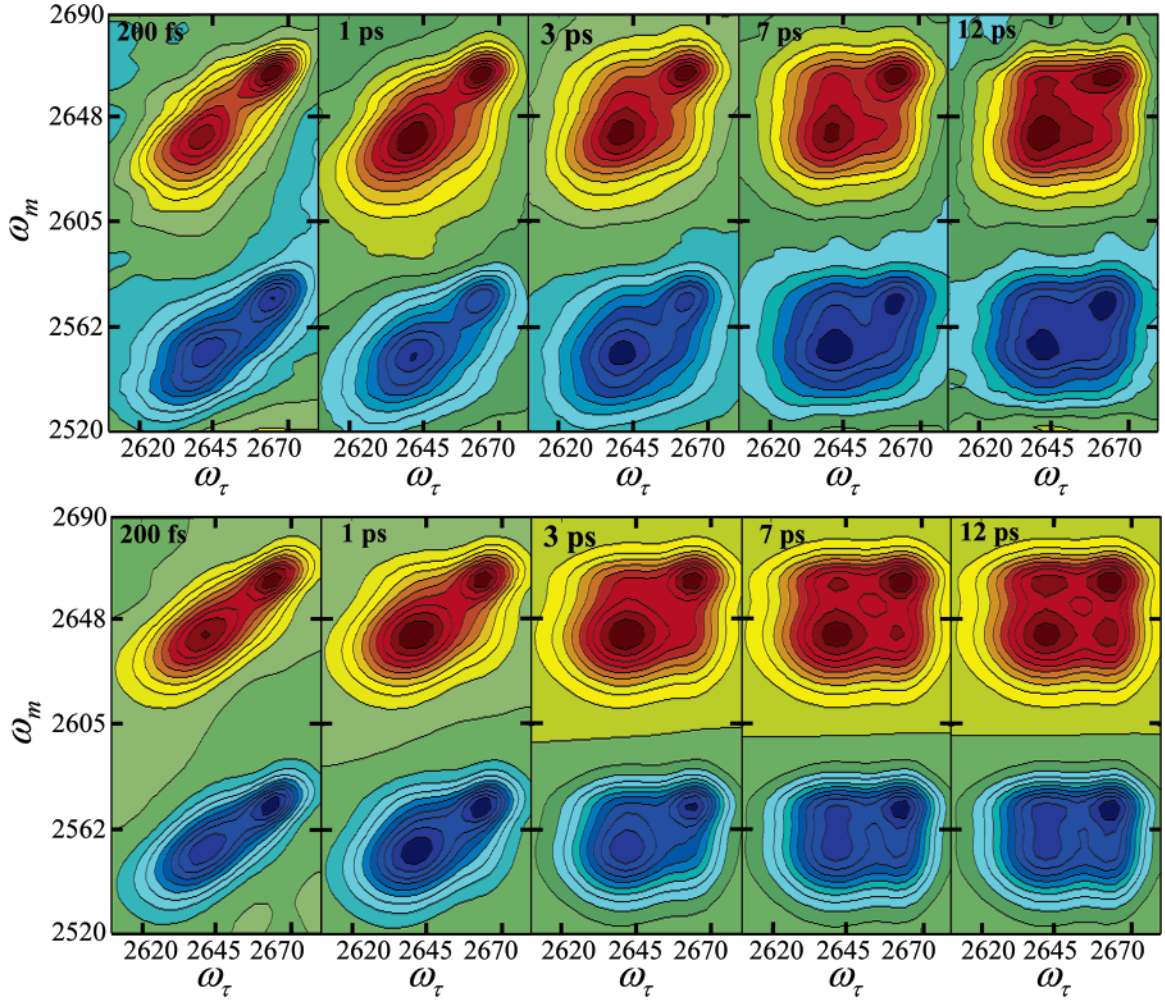

Figure 6. T_w-dependent 2D IR vibrational echo spectra (top) of the hydroxyl stretch of phenol-OD in bromobenzene/CCl_4 mixed solvents (molar ratio of phenol/bromobenzene/CCl_4 = 2:98:100). The red peaks (positive) are from the 0−1 vibration transitions, and the blue peaks (negative) are from the 1−2 vibrational transitions. At 200 fs, there are two peaks on the diagonal (red) and two peaks below these (blue) shifted by the anharmonicity. As T_w increases, additional peaks appear due to chemical exchange, that is, dissociation and formation of the phenol−bromobenzene complex. The bottom portion displays response function calculations of the data.

and the proper analysis, there is only one adjustable parameter, the dissociation time, τ_d.

One aspect of the volume fitting method is worth noting. The phenol−bromobenzene system has a linear spectrum in which the peaks are only slightly separated (Figure 7a). The result is that the diagonal and off-diagonal peaks in the 2D spectra have a great deal of overlap (Figure 6, top). The substantial overlap makes it tricky to extract the peak volumes in Figure 7c, particularly of the off-diagonal peaks. Nonetheless, there is sufficient accuracy to obtain the complex dissociation time with the same value as the full response function analysis. Note that the set of off-diagonal peak volumes extracted from the full response function calculations actually falls on the curve obtained by the peak volume fitting method (Figure 7b) better than points obtained by straight peak volume fitting (Figure 7c). Therefore, for systems such as bromobenzene, the full response function approach may give more accurate results in some instances.

VII. Concluding Remarks

Ultrafast 2D IR vibrational echo chemical exchange data were presented for the fast dissociation and formation of three organic solute−solvent complexes under thermal equilibrium conditions, and a detailed theoretical treatment of the 2D IR vibrational echo chemical exchange observables was presented. The experimental 2D spectral data, taken on the phenol hydroxyl stretching mode for three solute−solvent complexes (phenol/benzene, phenol/*p*-xylene, and phenol/bromobenzene), were analyzed using the theory. The theory includes the important dynamical processes of orientational relaxation, vibrational lifetime, and spectral diffusion in addition to the chemical exchange itself. The orientational relaxation, vibrational relaxation, and exchange process are introduced through the dynamic partition model (eq 11), which gives the kinetic equations for the effective population as a function of time. The effective population includes the decrease in signal caused by orientational relaxation. The difficulty in handling orientational relaxation and vibrational relaxation is caused by the fact that the two species undergo these relaxation processes at different rates. A species begins relaxation with certain rates, converts to the other species, and continues to relax with different rates. It then can revert to the initial species and relax further with the original rates and so on.

The analytical results of the dynamic partition model were then used with a time-dependent diagrammatic perturbation theory treatment to obtain analytical expressions for the response functions with exchange, spectral diffusion, orientational relaxation, and vibrational relaxation. Quantum pathways for

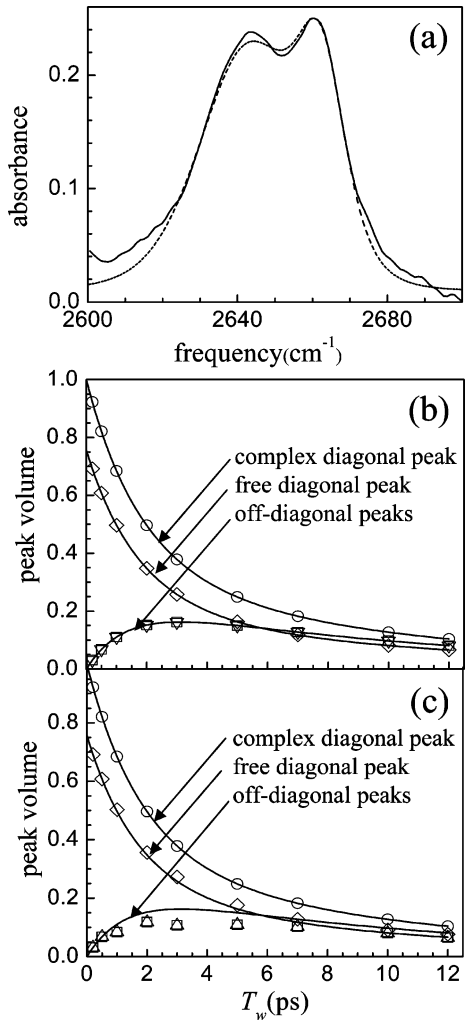

Figure 7. (a) Spectrum of the hydroxyl stretch of phenol-OD in the bromobenzene/CCl_4 mixed solvent (solid curve) and the calculated spectrum (dashed curve). The high-frequency peak is the free phenol, and the low-frequency peak is the phenol−bromobenzene complex. The calculated spectrum used the FFCF obtained by fitting the 2D vibrational echo spectra (Figure 6, bottom). (b) The points are peak volumes obtained from the response function calculations. The solid curves were obtained from fits using the peak volume method discussed in section VI. (c) The points are peak volumes obtained by fitting the 2D vibrational echo spectra (Figure 6, top) using the peak volume method (section VI). The solid curves are fits to the peak volumes.

diagonal peaks were divided into two classes, no exchange and multiple exchanges, because these two classes of pathways show different T_w-dependent line broadening. The line broadening of the portion of the diagonal peaks that undergo no exchange is determined by the spectral diffusion. However, the T_w-dependent line broadening from the pathways with multiple exchanges (an even number) is the result of the chemical exchange itself. To properly account for the T_w-dependent shape of the diagonal peaks and obtain the FFCF, it is necessary to separate the two contributions to the diagonal peak broadening.

Because a large number of the necessary input parameters were measured independently (Table 2), the only adjustable parameters in the calculations of the 2D spectra were the exchange rate and the FFCF. The calculations reproduced 2D IR vibrational echo spectra very well for all three species (Figures 1, 4, and 6), yielding exchange rates and the FFCF parameters of both the phenol complex and the free phenol for each of the three systems (Table 3). There is a marked difference in the spectral diffusion of the complex and the free species. The free species reflects the influence of solvent fluctuations on the hydroxyl stretch frequency. For the complexes, there is an additional contribution from the relative motions of the phenol and its complex partner.

The results of the full response function calculations were compared to those of the previously employed peak volume fitting method. The peak volume method does not determine the spectral diffusion because it fits the time-dependent peak volumes without analyzing the change in shapes of the peaks. However, it can be used to extract the exchange rate from the 2D data but does not determine the FFCF. Comparisons to the full response function calculations show that the simpler to implement peak volume method is accurate and a reasonable approach to obtain the exchange rate information.

Acknowledgment. This research was supported by grants from the Air Force Office of Scientific Research (F49620-01-1-0018) and from the National Science Foundation (DMR-0332692).

Appendix

In eqs 11, the detailed solutions of dynamic partition model were given. Here, the various symbols used in the equation are defined.

$$\alpha = \frac{D_c + D_f + k_c + k_f + k_{cf} + k_{fc}}{2}$$

$$\beta = \frac{\sqrt{(D_c + D_f + k_c + k_f + k_{cf} + k_{fc})^2 - 4(D_cD_f + D_fk_c + D_fk_{cf} + D_ck_f + k_ck_f + k_{cf}k_f + D_ck_{fc} + k_ck_{fc})}}{2}$$

$$\gamma = \frac{(D_c + D_f + k_c + k_f + k_{cf} + k_{fc}) - 2(D_f + k_f + k_{fc})}{\sqrt{(D_c + D_f + k_c + k_f + k_{cf} + k_{fc})^2 - 4(D_cD_f + D_fk_c + D_fk_{cf} + D_ck_f + k_ck_f + k_{cf}k_f + D_ck_{fc} + k_ck_{fc})}}$$

$$\phi = \frac{k_c + k_{cf} + k_f + k_{fc}}{2}$$

$$\varphi = \frac{\sqrt{(k_c + k_{cf} + k_f + k_{fc})^2 - 4(k_ck_f + k_{cf}k_f + k_ck_{fc})}}{2}$$

$$\theta = \frac{(k_c + k_{cf} + k_f + k_{fc}) - 2(k_f + k_{fc})}{\sqrt{(k_c + k_{cf} + k_f + k_{fc})^2 - 4(k_ck_f + k_{cf}k_f + k_ck_{fc})}}$$

References and Notes

(1) Zheng, J.; Kwak, K.; Asbury, J. B.; Chen, X.; Piletic, I.; Fayer, M. D. *Science* **2005**, *309*, 1338.

(2) Zheng, J.; Kwak, K.; Chen, X.; Asbury, J. B.; Fayer, M. D. *J. Am. Chem. Soc* **2006**, *128*, 2977.

(3) Schneider, H.-J.; Yatsimirsky, A. K. *Principles and Methods in Supramolecular Chemistry*; John Wiley & Sons: New York, 2000.

(4) Meyer, E. A.; Castellano, R. K.; Diederich, F. *Angew. Chem., Int. Ed.* **2003**, *42*, 1210.

(5) Vinogradov, S. N.; Linnell, R. H. *Hydrogen Bonding*; Van Nostrand Reinhold: New York, 1971.

(6) Reichardt, C. *Solvents and Solvent Effects in Organic Chemistry*; Wiley-VCH: Weinheim, Germany, 2003.

(7) Fayer, M. D.; Zheng, J.; Kwak, K.; Asbury, J. B. Molecular Dynamics/Theoretical Chemistry Meeting, May, 2005, Monterey, California.

(8) Kim, Y. S.; Hochstrasser, R. M. *Proc. Natl. Acad. Sci. U.S.A.* **2005**, *102*, 11185.

(9) Woutersen, S.; Mu, Y.; Stock, G.; Hamm, P. *Chem. Phys.* **2001**, *266*, 137.

(10) Dunand, F. A.; Helm, L.; Merbach, A. E. *Adv. Inorg. Chem.* **2003**, *54*, 1.
(11) Strehlow, H. *Rapid Reactions in Solutions*; VCH Publishers: New York, 1992.
(12) Wood, K. A.; Strauss, H. L. *J. Phys. Chem.* **1990**, *94*, 5677.
(13) Wood, K. A.; Strauss, H. L. *Ber. Bunsen-Ges.* **1989**, *93*, 615.
(14) Levinger, N. E.; Davis, P. H.; Behera, P.; Myers, D. J.; Stromberg, C.; Fayer, M. D. *J. Chem. Phys.* **2003**, *118*, 1312.
(15) Jeener, J.; Meier, B. H.; Bachmann, P.; Ernst, R. R. *J. Chem. Phys.* **1979**, *71*, 4546.
(16) Meier, B. H.; Ernst, R. R. *J. Am. Chem. Soc.* **1979**, *101*, 6441.
(17) Palmer, A. G. *Chem. Rev.* **2004**, *104*, 3623.
(18) Demirdoven, N.; Khalil, M.; Golonzka, O.; Tokmakoff, A. *J. Phys. Chem. A* **2001**, *105*, 8030.
(19) Zanni, M. T.; Hochstrasser, R. M. *Curr. Opin. Struct. Biol.* **2001**, *11*, 516.
(20) Golonzka, O.; Khalil, M.; Demirdoven, N.; Tokmakoff, A. *Phys. Rev. Lett.* **2001**, *86*, 2154.
(21) Merchant, K. A.; Thompson, D. E.; Fayer, M. D. *Phys. Rev. Lett.* **2001**, *86*, 3899.
(22) Volkov, V.; Schanz, R.; Hamm, P. *Opt. Lett.* **2005**, *30*, 2010.
(23) Zanni, M. T.; Gnanakaran, S.; Stenger, J.; Hochstrasser, R. M. *J. Phys. Chem. B* **2001**, *105*, 6520.
(24) Asbury, J. B.; Steinel, T.; Stromberg, C.; Gaffney, K. J.; Piletic, I. R.; Goun, A.; Fayer, M. D. *Phys. Rev. Lett.* **2003**, *91*, 237402.
(25) Steinel, T.; Asbury, J. B.; Corcelli, S. A.; Lawrence, C. P.; Skinner, J. L.; Fayer, M. D. *Chem. Phys. Lett.* **2004**, *386*, 295.
(26) Asbury, J. B.; Steinel, T.; Fayer, M. D. *Chem. Phys. Lett.* **2003**, *381*, 139.
(27) Zheng, J.; Kwak, K.; Steinel, T.; Asbury, J. B.; Chen, X.; Xie, J.; Fayer, M. D. *J. Chem. Phys.* **2005**, *123*, 164301.
(28) Khalil, M.; Demirdoven, N.; Tokmakoff, A. *J. Phys. Chem. A.* **2003**, *107*, 5258.
(29) Kim, Y.; Hochstrasser, R. M. *J. Phys. Chem. B.* **2005**, *109*, 6884.
(30) Mukamel, S. *Principles of Nonlinear Optical Spectroscopy*; Oxford University Press: New York, 1995.
(31) Knee, J. L.; Khundkar, L. R.; Zewail, A. H. *J. Chem. Phys.* **1987**, *87*, 115.
(32) Perutz, M. F. *Philos. Trans. R. Soc. London, Ser. A* **1993**, 105.
(33) Trebino, R.; DeLong, K. W.; Fittinghoff, D. N.; Sweetser, J. N.; Krumbugel, M. A.; Richman, B. A.; Kane, D. J. *Rev. Sci. Instrum.* **1997**, *69*, 3277.
(34) Khalil, M.; Demirdoven, N.; Tokmakoff, A. *Phys. Rev. Lett.* **2003**, *90*, 047401.
(35) Asbury, J. B.; Steinel, T.; Fayer, M. D. *J. Lumin.* **2004**, *107*, 271.
(36) Jonas, D. M. *Annu. Rev. Phys. Chem.* **2003**, *54*, 425.
(37) Woutersen, S.; Mu, Y.; Stock, G.; Hamm, P. *Proc. Natl. Acad. Sci. U.S.A.* **2001**, *98*, 11254.
(38) Woutersen, S.; Bakker, H. J. *Nature* **1999**, *402*, 507.
(39) Gaffney, K. J.; Piletic, I. R.; Fayer, M. D. *J. Chem. Phys.* **2003**, *118*, 2270.
(40) Jasen, J.; Hayashi, T.; Zhuang, W.; Mukamel, S. *J. Chem. Phys.* **2005**, *123*, 114504.
(41) Kwac, K. L.; H. Cho, M. *J. Chem. Phys.* **2004**, *120*, 1477.
(42) Kubo, R. A Stochastic Theory of Line-Shape and Relaxation. In *Fluctuation, Relaxation and Resonance in Magnetic Systems*; Ter Haar, D., Ed.; Oliver and Boyd: London, 1961.
(43) Carrington, A.; McLachlan, A. D. *Introduction to Magnetic Resonance*; Harper and Row: New York, 1967.
(44) Asbury, J. B.; Steinel, T.; Fayer, M. D. *J. Phys. Chem. B.* **2004**, *108*, 6544.
(45) Bain, A. D. *Prog. Nucl. Magn. Reson. Spectrosc.* **2003**, *43*, 63.
(46) Kubo, R. *J. Phys. Soc. Jpn.* **1954**, *9*, 935.
(47) Sack, R. A. *Mol. Phys.* **1958**, *1*, 163.
(48) Tokmakoff, A. *J. Chem. Phys.* **1996**, *105*, 1.
(49) McQuarrie, D. A. *Statistical Mechnics*; Haper-Collins: New York, 1973.
(50) Putzer, E. J. *Am. Math. Mon.* **1966**, *73*, 2.
(51) Mukamel, S. *Annu. Rev. Phys. Chem.* **2000**, *51*, 691.
(52) Stenger, J.; Madsen, D.; Hamm, P.; Nibbering, E. T. J.; Elsaesser, T. *J. Phys. Chem. A.* **2002**, *106*, 2341.